NAVAL POSTGRADUATE SCHOOL
Monterey, California

THESIS

QUANTITATIVE ENERGY DISPERSIVE X-RAY SPECTROMETRY USING AN EMISPEC VISION SYSTEM

by

Carlos A. Kasemodel

December 1999

Thesis Advisor: Alan G. Fox
Co-Advisor: James Luscombe

Approved for public release; distribution is unlimited.

REPORT DOCUMENTATION PAGE

Form Approved
OMB No. 0704-0188

1. AGENCY USE ONLY *(Leave blank)*	2. REPORT DATE	3. REPORT TYPE AND DATES COVERED
	December 1999	Master's Thesis

4. TITLE AND SUBTITLE:
QUANTITATIVE ENERGY DISPERSIVE X-RAY SPECTROMETRY USING AN EMISPEC VISION SYSTEM

5. FUNDING NUMBERS

6. AUTHOR(S)
Kasemodel, Carlos A.

7. PERFORMING ORGANIZATION NAME(S) AND ADDRESS(ES)
Naval Postgraduate School
Monterey, CA 93943-5000

8. PERFORMING ORGANIZATION REPORT NUMBER

9. SPONSORING / MONITORING AGENCY NAME(S) AND ADDRESS(ES)

10. SPONSORING/MONITORING AGENCY REPORT NUMBER

11. SUPPLEMENTARY NOTES
The views expressed here are those of the authors and do not reflect the official policy or position of the Department of Defense or the U.S. Government.

12a. DISTRIBUTION / AVAILABILITY STATEMENT
Approved for public release; distribution is unlimited.

12b. DISTRIBUTION CODE

13. ABSTRACT ***(maximum 200 words)***

The purpose of this work was to investigate the use of an Emispec Vision system to analyze energy dispersive x-ray spectra (EDS) obtained with the Topcon 002B transmission electron microscope (TEM) in the Materials Science Laboratory at the Naval Postgraduate School.

A series of tests performed with a standard NiO sample revealed that the TEM column and EDS detector were operating in a satisfactory fashion. NiO spectra acquired with different sample tilt-angles were used to test the Emispec software. An improved setup configuration, in which accurate quantification is obtained with the sample at zero tilt-angle, was developed.

Quantification tests performed with TiO_2, Cu-Al_2O_3 and alumina-YAG (with 2.5% TiO_2) samples confirmed the accuracy of the new software setup. Line profiles across the alumina-YAG interfaces were also recorded to verify the performance of the Emispec system for spectrum profile acquisition and to investigate the Ti distribution at the interface of the alumina-YAG heat-treated sample.

14. SUBJECT TERMS	15. NUMBER OF PAGES
Transmission Electron Microscopy, Energy Dispersive X-Ray Spectra, EDS Quantitative Analysis	81
	16. PRICE CODE

17.SECURITY CLASSIFICATION OF REPORT	18.SECURITYCLASSIFICATION OF THIS PAGE	19. SECURITY CLASSIFICATION OF ABSTRACT	20. LIMITATION OF ABSTRACT
Unclassified	Unclassified	Unclassified	UL

NSN 7540-01-280-5500

Standard Form 298 (Rev. 2-89)
Prescribed by ANSI Std. 239-18 298-102

Approved for public release; distribution is unlimited

QUANTITATIVE ENERGY DISPERSIVE X-RAY SPECTROMETRY USING AN EMISPEC VISION SYSTEM

Carlos A. Kasemodel
Major, Brazilian Air Force
B.S., Instituto Tecnológico de Aeronáutica, Brazil, 1980

Submitted in partial fulfillment of the
requirements for the degree of

MASTER OF SCIENCE IN APPLIED PHYSICS

from the

NAVAL POSTGRADUATE SCHOOL
December 1999

Author:

Carlos A. Kasemodel

Approved by:

Alan G. Fox, Thesis Advisor

James Luscombe, Co-Advisor

Nagarajan Rajagopalan, Second Reader

William B. Maier II, Chairman
Department of Physics

ABSTRACT

The purpose of this work was to investigate the use of an Emispec Vision system to analyze energy dispersive x-ray spectra (EDS) obtained with the Topcon 002B transmission electron microscope (TEM) in the Materials Science Laboratory at the Naval Postgraduate School.

A series of tests performed with a standard NiO sample revealed that the TEM column and EDS detector were operating in a satisfactory fashion. NiO spectra acquired with different sample tilt-angles were used to test the Emispec software. An improved setup configuration, in which accurate quantification is obtained with the sample at zero tilt-angle, was developed.

Quantification tests performed with TiO_2, Cu-Al_2O_3 and alumina-YAG (with 2.5% TiO_2) samples confirmed the accuracy of the new software setup. Line profiles across the alumina-YAG interfaces were also recorded to verify the performance of the Emispec system for spectrum profile acquisition and to investigate the Ti distribution at the interface of the alumina-YAG heat-treated sample.

TABLE OF CONTENTS

ACKNOWLEDGMENT

The author would like to thank Dr. Alan G. Fox, Dr. James Luscombe and Dr. Sarath Menon for help and guidance during the course of this work.

A very special thanks is due to Dr. Nagarajan Rajagopalan for guidance, dedication and contribution of many hours of laboratory assistance.

I. INTRODUCTION

Transmission Electron Microscopy (TEM) is an extremely important technique in the field of materials characterization providing information down to the atomic level. The strength of TEM is that not only can it provide high-resolution images but it can also operate with small probes in various microanalytical modes due to the fact that a variety of signals are generated when an electron beam interacts with matter. Electron energy-loss and x-ray spectroscopy are examples of techniques which increase the potential of a conventional transmission electron microscope (CTEM) and transform it into an analytical electron microscope (AEM).

Advances in computers in recent years have brought many benefits to the area of electron microscopy and, today, a modern TEM always works with one or more computers in parallel, which perform many functions such as control, data acquisition and analysis. In addition, many packages of hardware and software are available to improve the computer capabilities, making life easier for the electron microscopist.

Recently, the Materials Science Laboratory at the Naval Postgraduate School has installed a new computational tool, called the Emispec Vision System, to operate in conjunction with the Topcon 002B TEM, monitoring mainly the functions of X-ray Energy-Dispersive Spectrometry (EDS). Despite the power of this modern system, the first results obtained in x-ray quantitative analysis were inaccurate and the object of this thesis was to investigate the origin of these inaccuracies.

Basically, the work was developed with the objective of answering the following questions:

- Is the Topcon 002B operating in an optimum fashion for EDS analysis?
- Is the Emispec system set up properly?
- Does the Emispec software work properly?

In order to meet these goals a series of tests were performed with a NiO standard sample to verify the work conditions of the TEM column and x-ray detector. This sample was also used to test modifications in the software setup and to establish procedures for EDS quantification. TiO_2, Cu-Al_2O_3 and Al_2O_3-$Y_3Al_5O_{12}$ (alumina-YAG) samples were also used to verify the capability to the Emispec system to perform quantitative analysis. The alumina-YAG sample was investigated more deeply and quantification of a spectrum profile across an alumina-YAG interface was performed.

II. BACKGROUND

A. TRANSMISSION ELECTRON MICROSCOPY

The Transmission Electron Microscope (TEM) was first developed in the 1930's after it was apparent that electrons behaved as waves with a wavelength much smaller than light. The idea being that small wavelength leads to improved resolution in images.

Basically, a conventional transmission electron microscope is an electron accelerator that focuses the electron beam onto a thin specimen with the aid of electromagnetic lenses. The illumination source, also known as the electron gun, emits electrons either by thermionic or field emission depending on the type of emitter installed. Condenser lenses demagnify the electron source and focus the electron beam onto the sample and objective, intermediate and projector lenses magnify the image after the electrons have passed through the specimen. A two- or three-stage condenser-lens system permits variation of the illumination aperture and of the area of the specimen illuminated. The electron intensity distribution behind the specimen is imaged with a three- or four-stage lens system onto a fluorescent screen.

The accelerating voltage of routine instruments is 80-120 kV. Intermediate voltage instruments work at 200-500 kV to provide a better transmission and resolution, and high-voltage instruments operate with accelerating potentials between 500 kV and 3 MV. Although the resolution improves with accelerating voltage, the theoretical

resolution is never reached because the lens aberrations are so great and it is necessary to work with very small objective apertures.

A schematic of a TEM is shown in Figure 2-1. The lenses and the specimen stage are mounted in a vertical, cylindrical column that is maintained under a vacuum of about 10^{-5} Pa. The vacuum is needed so that the electrons have a large mean free path between collisions with air molecules.

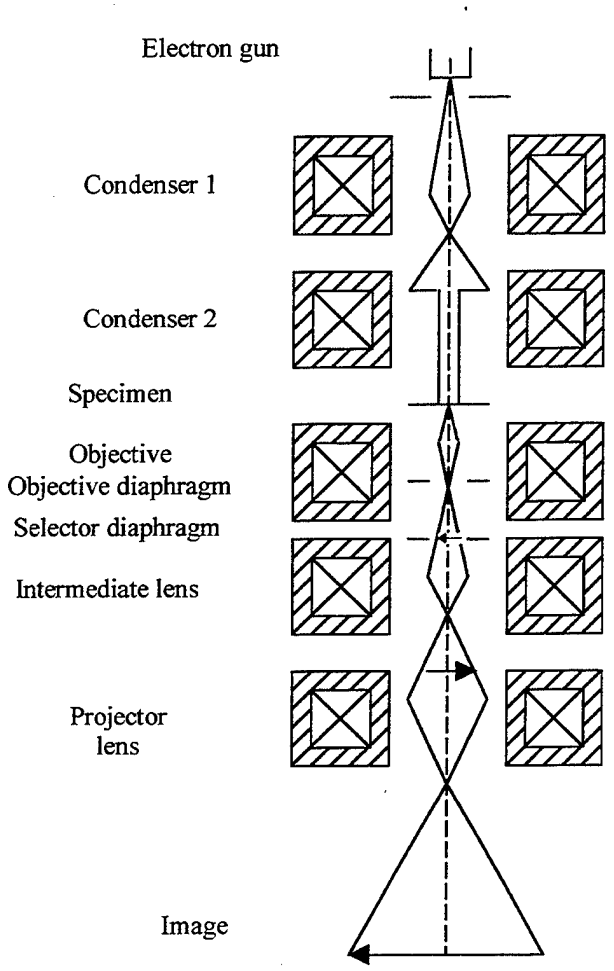

Figure 2-1. Schematic of a TEM [After Ref. 1].

Electron scattering is the process that makes TEM feasible. When a high-energy beam of electrons traverse through a thin foil material, a number of excitations result from the interactions between the incident beam and the atoms in the sample. Some electrons travel straight through the sample or are absorbed and do not provide useful information, but others interact strongly with atoms by elastic and inelastic scattering. These latter electrons, as well as other signals produced are the source of information in electron microscopy.

Figure 2-2 illustrates the main signals generated. Backscattered electrons are high-energy electrons emitted from the specimen as a result of elastic interactions between the incident beam and tightly bonded electrons within the specimen. Secondary electrons are weakly bonded electrons that are ejected by the incident beam. Characteristic x-rays are the emission of electromagnetic radiation due to interactions between the incident beam and inner-shell electrons. Bremsstrahlung x-rays are emitted when the electrons in the beam are decelerated due to interactions with the nucleus of an atom. Auger electrons can also be emitted instead of x-ray emission.

In TEM the signals of interest are those that go through the specimen. Backscattered and secondary electrons are of interest in scanning electron microscopy (SEM). Electrons that are scattered elastically in the forward direction are the most important of the interactions that contribute to image contrast. Inelastically scattered electrons and characteristic x-rays are used in Electron Energy Loss Spectrometry (EELS) and X-ray Energy-Dispersive Spectrometry (EDS), respectively. From these signals a lot of detail about the sample chemistry can be obtained.

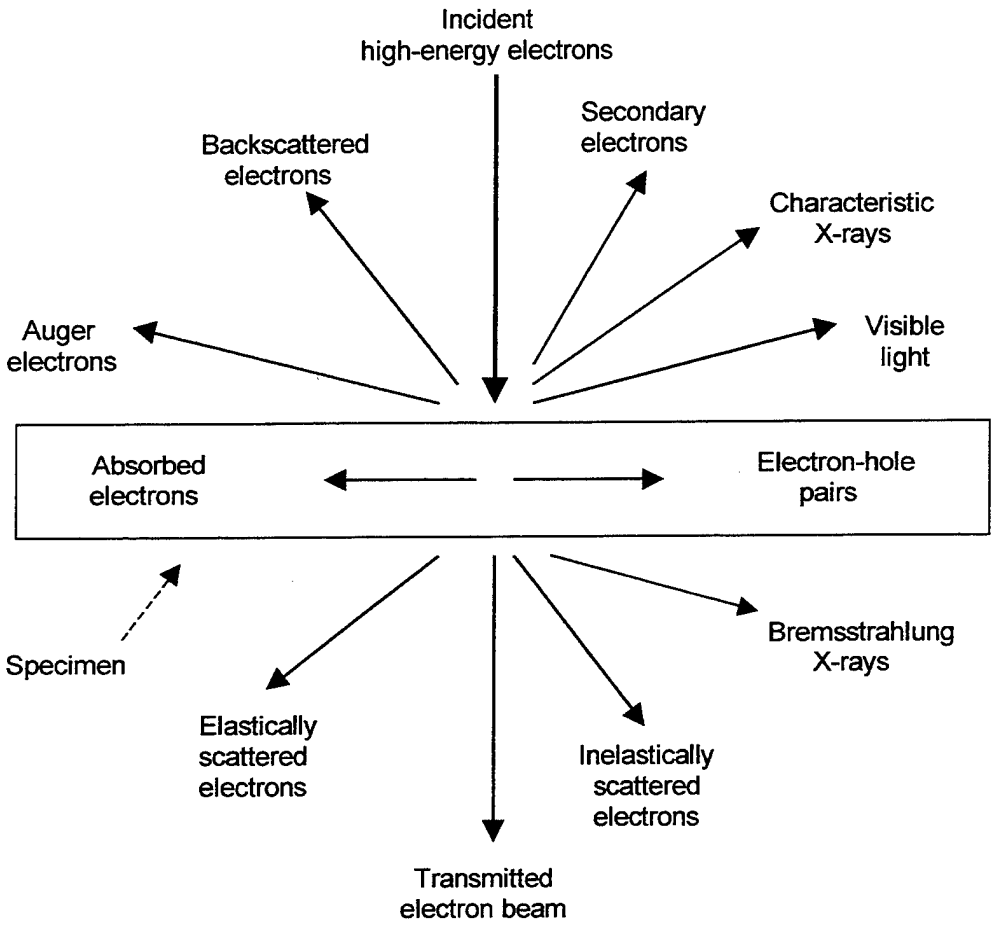

Figure 2-2. Signals generated when a high-energy beam of electrons interacts with a thin foil material [After Ref. 2].

B. ENERGY DISPERSIVE X-RAY ANALYSIS

1. General

In EDS, the x-rays produced by the interactions of the electron beam with the specimen are detected by a solid-state detector and analyzer producing an energy spectrum which is a plot of x-ray counts versus x-ray energy.

In general, an energy-dispersive x-ray spectrometer consists of three main parts: a detector, a pulse processor and a multi-channel analyzer and display. All the three parts are controlled by a computer as shown in Figure 2-3. The detector collects the x-rays and generates a pulse proportional to the x-ray energy. This pulse is converted to a voltage, amplified, identified electronically as resulting from an x-ray of specific energy and finally a digitized signal is stored in a channel assigned to that energy and displayed as a spectrum on a computer screen.

A typical spectrum is shown on Figure 2-4. It consists of a number of peaks superimposed on a slowly varying continuous background. The peaks are produced by characteristic x-rays and the background by Bremsstrahlung x-rays. Although the natural energy spread of the x-rays in a particular emission line is very small, the x-ray line is recorded as a Gaussian distribution several tens of eV wide because of noise in the detector and amplifier system.

The characteristic x-rays are those that contain the useful information, such as elemental composition. The mechanism by which they are produced is presented in more detail in the next section.

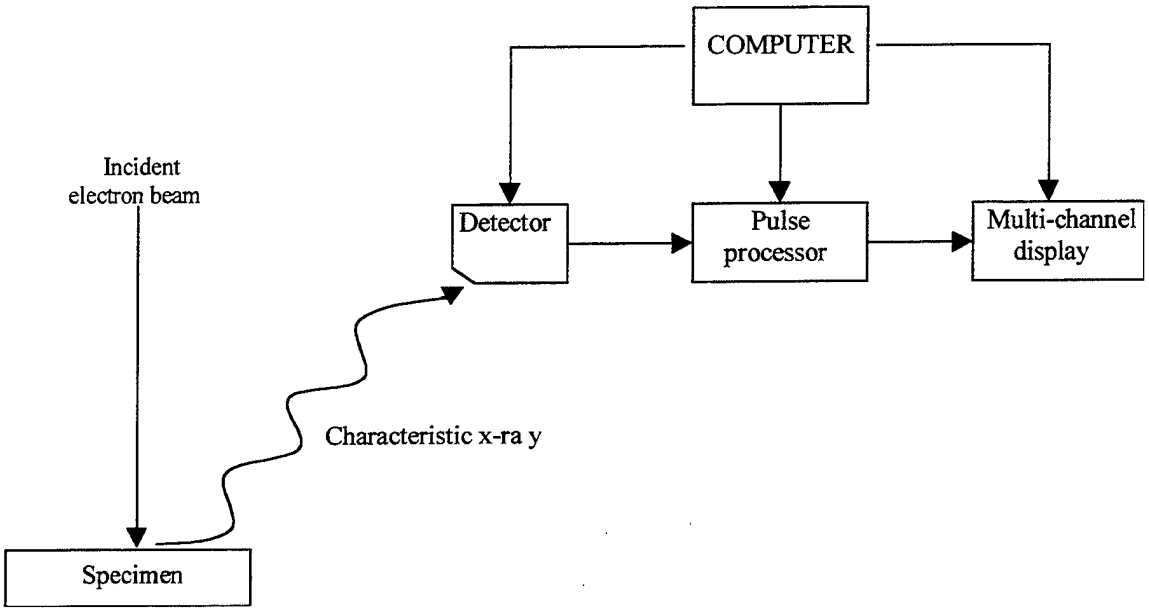

Figure 2-3. Diagram of the EDS System.

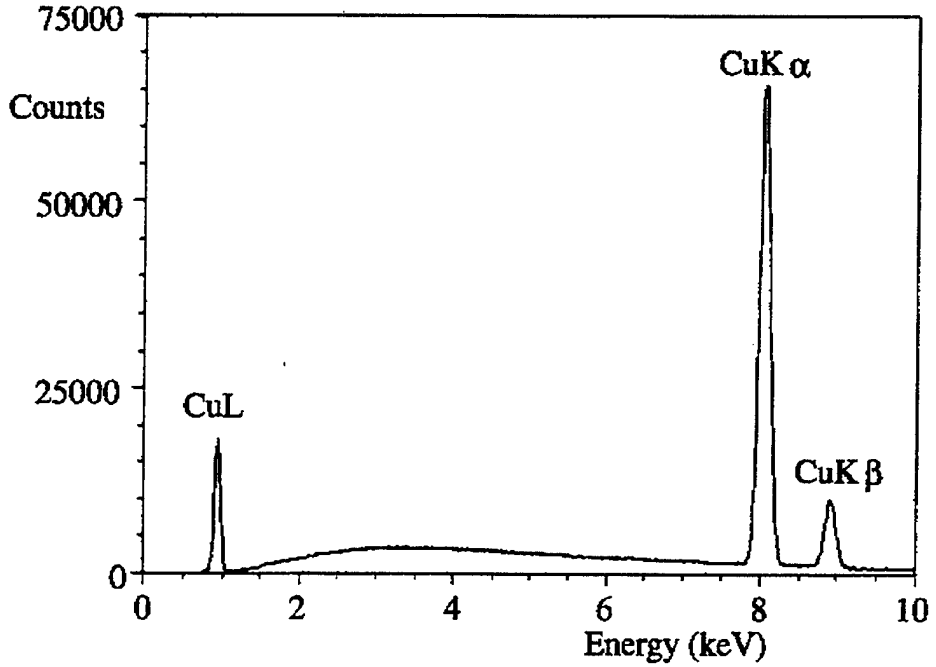

Figure 2-4. Typical EDS Spectrum [From Ref. 3].

2. Characteristic X-Rays

To understand the production of characteristic x-rays it is necessary to invoke the Bohr theory of atomic structure in which the electrons are orbiting the nucleus in specific shells. The innermost shell of electrons is the K shell, the next innermost one the L shell, the next one the M shell, and so on.

If the incident beam of electrons hitting an atom in the sample has sufficient energy to eject an inner-shell electron, the atom will be left in an excited state with a hole in that shell. When an electron from an outer shell fills this hole, an x-ray photon, with an

energy equal to the difference in the electron energy levels, can be produced. The energy of this photon is characteristic of that specific atom in the sample and, for this reason, is called a characteristic x-ray. Instead of producing a characteristic x-ray, the ionized atom can emit an Auger electron. The probability of x-ray emission versus Auger electron emission is described by the fluorescence yield, ω, which is the ratio of the number of x-ray photons emitted to the total number of inner shell ionizations [Ref. 2].

The notation used for identifying the characteristic x-rays is a little complicated. When a hole in the K shell is filled with an electron from the L shell, a K_α x-ray is produced, but if it is filled with an electron from the M shell, a K_β x-ray is produced. If the hole is in the L shell and it is filled with an electron from the M shell, an L_α x-ray is emitted. Figure 2-5 shows schematically the origin of these characteristic transitions.

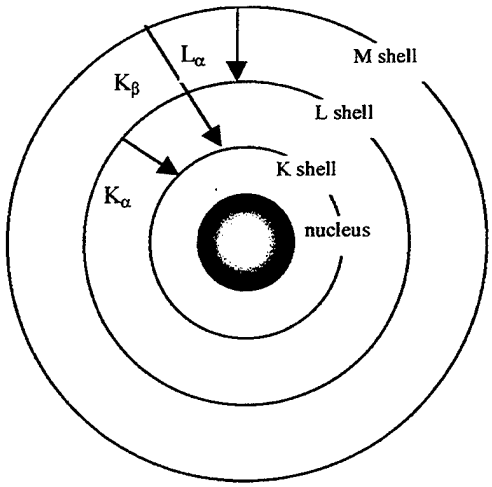

Figure 2-5. Electron transitions in an atom and the production of characteristic x-rays [After Ref. 4].

The situation is more complex due to the presence of the sub-shells, for example, a K_α x-ray line actually contains two lines, $K_{\alpha 1}$ and $K_{\alpha 2}$. The reason for this is that the L shell consists of three sub-shells, L_I, L_{II} and L_{III}. A transition from L_{III} to K results in the emission of the $K_{\alpha 1}$ x-ray and a transition from L_{II} to K results in the emission of the $K_{\alpha 2}$ x-ray. It is not always possible to resolve the $K_{\alpha 1}$ and $K_{\alpha 2}$ peaks in the spectrum because the energies are so close and, in this case, the characteristic peak is simply called K_α. Also, not all electron transitions are possible. The absence of certain transitions is based on specific selection rules that result from the solution of the Schrödinger equation. The solution of this equation for any element allows the energy levels (shells) for that element to be predicted.

3. EDS Detectors

The type of detector used in EDS is essentially a reverse-biased p-i-n semiconductor diode. When x-rays interact with a semiconductor, the primary method of energy deposition is the transfer of electrons from the valence band to the conduction band, creating electron-hole pairs. Due to the reverse bias applied to the crystal, the electrons and holes are separated and a charge pulse of electrons can be measured. The magnitude of this pulse is proportional to the energy of the x-ray that generated the electron-hole pairs.

The intrinsic region of the detector is called as the "active layer" and the p and n regions are called the "dead layers", since the electron-hole pairs generated in these regions recombine, and contribute nothing to the charge pulse. However, in practice, it is

the layer at the entrance surface of the detector, which x-rays must traverse to be detected, that is called "dead layer".

Two types of detector are generally used, a lithium drifted silicon (Si-Li) detector or an intrinsic germanium (IG) detector. Both types have advantages and disadvantages. IG detectors are frequently used in intermediate voltage AEMs, because Si-Li detectors present a drop in efficiency above 20 keV and IG detectors are able to absorb these high-energy x-rays.

For good performance, the detector must be kept at a low temperature and the crystal surface must be maintained absolutely clean, which requires the operation in a high quality clean vacuum. For this reason, the detector is generally isolated from the microscope in a pre-pumped tube with a "window" to allow the entrance of x-rays. Different types of windows exist and the knowledge of their characteristics is of great importance. Older detectors use a thin foil of Beryllium, which strongly absorb the light element x-rays and chemical analysis of light elements then become impossible. Since the late 1980s, detectors have been fitted with alternative windows, usually made from very thin (<100 nm) films of polymer, diamond, boron nitrate or silicon nitrate, which are able to transmit light element x-rays. Windowless detectors have also been developed but they require operation in ultra-high vacua.

4. Sources of Error in EDS

The acquisition of quality results in EDS requires a knowledge of its limitations and an understanding of spectrum artifacts.

a. EDS Limitations

(1) Light Element Analysis. Quantitative analysis is very difficult for elements of atomic number less than 11. The highest energy of the emitted x-rays from these elements is about 1 keV and the detector efficiency is very poor at these energies. Also, they are strongly absorbed by some detector windows and the contact layers of the detector. In addition, the fluorescence yield for light element x-rays is very low so that the signal from these x-rays is very weak. Finally, these low-energy x-rays can be significantly absorbed by the sample so that careful absorption corrections are important.

(2) Energy Resolution. The energy resolution of a EDS detector is about 140 eV at the Mn-Kα characteristic line. When the elements in the specimen present characteristic x-rays with energies that overlap, the peaks are not resolved, which can result in errors in quantitative analysis.

(3) Dead-time. Dead time is the period of time that detector is switched off while the pulse-processor analyzes an incoming pulse. During this time, another x-ray cannot be processed. The dead time increases as more x-rays try to enter the detector and if the count rate is excessively high, the collection of x-rays becomes inefficient. Expressions for determination of the dead time can be obtained from Ref. 3 and a typical value for a Si(Li) detector is about 20-25%. This means that is advisable to

keep the number of counts per second generated in the detector at less than about 3,000 in order to maintain optimum energy resolution.

b. Spectrum Artifacts

(1) Spurious x-rays. Spurious x-rays can produce undesirable peaks in the spectrum and if they are presented in significant amounts, the quantification process can give wrong answers. Spurious x-rays can be divided into pre and post-specimen effects. Pre-specimen effects are stray x-rays produced by the illumination system due to the interaction of uncollimated electrons and the microscope column. Post-specimen effects are characteristic x-rays of the materials used to construct the sample holder, the sample support grid, etc, that arise due to interactions of scattered electrons with these materials.

(2) Escape Peaks. Escape peaks are caused by the fluorescence of x-rays within the detector by an incoming x-ray from the specimen. For example, in Si(Li) detectors, Si K_α x-rays (energy 1.74 keV) can fluoresce inside the detector and escape peaks will appear in the spectrum 1.74 keV below the characteristic peak position. Escape peaks, in general, are not a major problem because almost all analysis programs can identify and make corrections for them.

(3) Sum Peaks. Sum peaks are generated when two incoming characteristic x-rays of the same energy hit the detector with very close arrival times and the electronic circuitry does not detect that there are two. The result is the apparent detection of an x-ray with an energy equal to the sum of the two incident x-rays. With modern electronics, the sum peaks only become significant at very high-count rates.

(4) Coherent Bremsstrahlung. Coherent bremsstrahlung results from the interaction of the incident electrons with the periodic structure of crystalline specimens, and typically produces small peaks in the 1-4 keV region of the spectrum. It becomes important when searching for very low (<1%) concentrations of impurities.

5. Spatial Resolution in EDS

Knowledge of the spatial resolution in EDS becomes important when investigating very small sample features that are close in size to the probe diameter, since unwanted contributions from surroundings areas can affect the results.

Spatial resolution in EDS can be defined as the smallest distance between two volumes from which independent x-ray analysis can be obtained. This analysis volume is a function of the incident beam diameter (d) and the beam spreading (b) caused by elastic scatter of the beam within the specimen. An equation often used to determine the spatial resolution (R) is given by:

$$R = \frac{d + R_{max}}{2} \tag{2.1}$$

where,

$$R_{max} = (b^2 + d^2)^{1/2} \tag{2.2}$$

The beam spreading can be determined by the Reed model [Ref. 3]:

$$b = 7.21 \times 10^5 (\frac{Z}{E_o})(\frac{\rho}{A})^{1/2} t^{3/2} \qquad \text{(cm)} \tag{2.3}$$

where,

Z = atomic number

E_o = accelerating voltage (eV)

ρ = density (g/cm^3)

A = atomic weight

t = thickness (cm)

Since spatial resolution is a function of the incident beam diameter, d, AEMs equipped with field emission gun have a better resolution because they can produce a smaller probe diameter than the thermionic emission guns. For a LaB_6 emitter on the Topcon 002B at 200 kV, the smallest incident probe diameters that can be used to provide EDS spectra with satisfactory signal-to-noise ratios are in the range of 5-10 nm and so the limit of spatial resolution will be around 10-20 nm depending on the sample thickness and atomic number.

C. QUANTITATIVE X-RAY MICROANALYSIS

1. General

The possibility of using x-rays generated by a focused electron beam to give elemental information of a bulk specimen was first described by Hillier and Baker (1944), followed by Castaing (1951) [Ref. 3]. Castaing suggested that the concentration C_i of an element i in a specimen is proportional to the intensity of one of the peaks of its characteristic x-rays and, if a standard of composition $C_{(i)}$ for the element i is known, the composition C_i in the specimen can be determined by the following expression:

$$\frac{C_i}{C_{(i)}} = K\frac{I_i}{I_{(i)}} \tag{2.4}$$

where,

- I_i is the measured intensity of the chosen characteristic line emerging from the specimen,

- $I_{(i)}$ is the measured intensity of the chosen characteristic line emerging from the standard,

- K is a sensitivity factor that takes into account the difference between the generated and measured x-rays intensities for both the standard and unknown specimen.

The contributions to K come from three effects:

- The atomic number, Z
- The absorption of x-rays within the specimen, A
- The fluorescence of x-rays within the specimen, F

The K-factor is often referred to as the *ZAF* correction and equation 2.4 can be written as:

$$\frac{I_i}{I_{(i)}} = ZAF\frac{C_i}{C_{(i)}} \tag{2.5}$$

where Z, A, and F represent the atomic-number, absorption, and fluorescence corrections, respectively. If a thin electron transparent specimen is used rather than a bulk one, the *A* and *F* factors can often be ignored and only the *Z* correction is necessary.

2. The Cliff-Lorimer Method

Cliff and Lorimer (1975) showed that quantification is possible with a simple version of Castaing's original ratio equation in which there was no need to incorporate intensity data from a standard, but simply ratio the intensities gathered from two elements simultaneously in the EDS. The basis for the Cliff-Lorimer technique is to rewrite equation (2.4) for two elements A and B in a binary system. In this way, the weight percents of each element C_A and C_B can be related to the measured intensities as follows:

$$\frac{C_A}{C_B} = k_{AB}\frac{I_A}{I_B} \tag{2.6}$$

where k_{AB} is termed the Cliff-Lorimer k factor. For a binary system $C_A + C_B = 100\%$ and the absolute values of C_A and C_B can be determined.

These equations can be extended to ternary or higher order systems by writing extra equations of the form

$$\frac{C_B}{C_C} = k_{BC}\frac{I_B}{I_C} \tag{2.7}$$

$$C_A + C_B + C_C = 100\%$$

The Cliff-Lorimer k factor depends upon the elements being analyzed, the energy of the incident electrons and the sensitivity of the x-ray detector for the different x-rays. It can be shown [Ref. 3] that the Cliff-Lorimer k factor for thin-foil analysis is related to the atomic number correction factor Z, by the following equation:

$$k_{AB} = \frac{1}{Z} = \frac{(Q\omega a)_B A_A \varepsilon_A}{(Q\omega a)_A A_B \varepsilon_B} \tag{2.8}$$

where,

- Q is the ionization cross section,
- ω is the fluorescence yield for the characteristic x-rays,
- A is the atomic weight,
- a is the fraction of the K line (or L and M) which is collected,
- ε is the detector efficiency.

The Cliff-Lorimer equation is the basis for quantification microanalysis in AEM.

3. Background Subtraction

Determination of the peak intensities to be used in the quantification methods described in the previous sections requires the subtraction of the background intensity. This background is the intensity under the characteristic peaks and, as was mentioned earlier, is generated mainly by the Bremsstrahlung x-rays.

Different methods can be used to remove the background, the simplest being the selection of appropriate windows in the spectrum to estimate the intensity under the peak. Mathematical modeling approaches are also available and are most useful for multi-element spectra and those containing peaks below 1.5 keV.

III. EXPERIMENTAL PROCEDURE

A. INSTRUMENTATION

1. Transmission Electron Microscope

For the present work a TOPCON 002B TEM with a LaB_6 emitter energized to 200 kV was used. This TEM has a scanning capability and is equipped with an EDAX EDS system (model # PV9791/28) and the Emispec Vision System for data acquisition and analysis. Figure 3-1 shows a photograph of the microscope. The hardware in the right corner of the figure is the Emispec system.

2. EDS Detector

The EDS detector is a Si(Li) semiconductor detector equipped with a Moxtek ultra-thin window. The detector window is composed of 400 Å of aluminum and 3,000 Å of the Moxtek polymer AP1 ($C_{22}H_{12}O_5N_2$) [Ref. 6]. Table 3.1 presents some typical characteristics of the detector [Ref. 7].

Detector area	**30.0 mm^2**
Detector thickness	**3.0 mm**
Dead layer thickness	**85.0 nm**
Resolution	**139.5 eV (at 5.9 keV)**

Table 3-1. EDS Detector Characteristics.

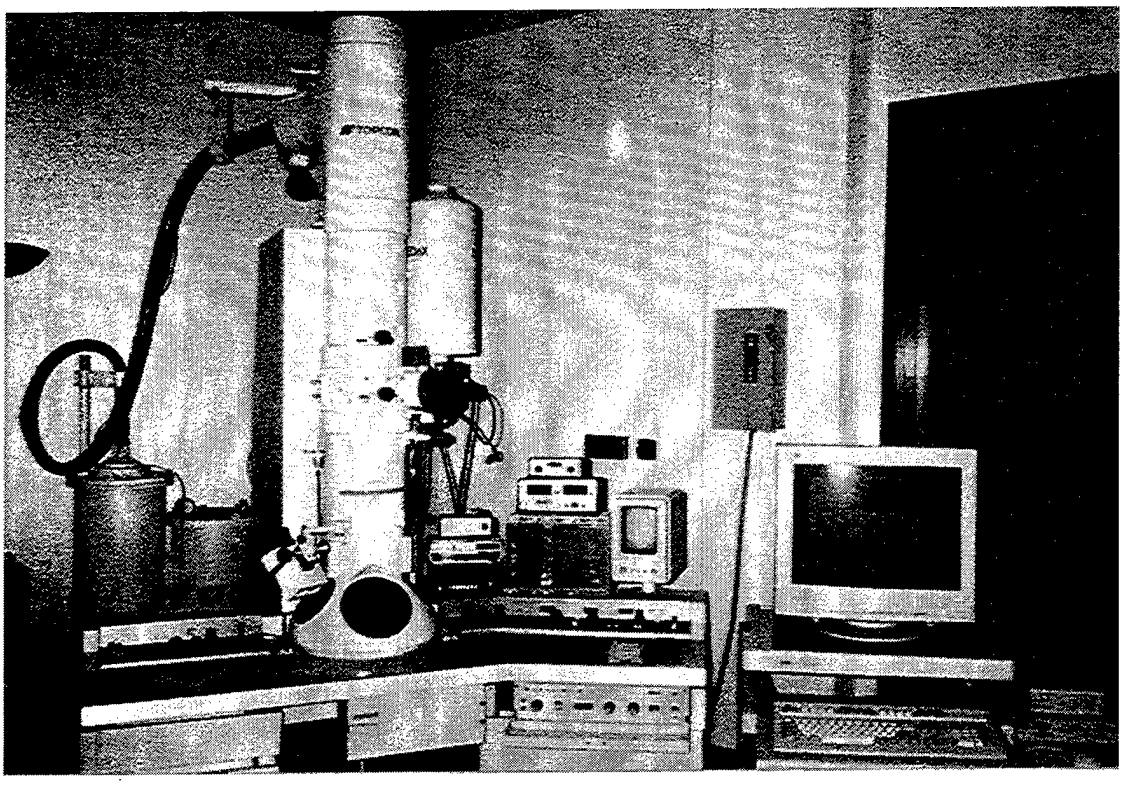

Figure 3-1. TOPCON 002B TEM.

3. Emispec Vision System

The Emispec Vision System is a combination of computer hardware and software designed to perform a variety of complex experiments in digital electron microscopy. The system is modular and its performance depends on the modules used and the detectors installed in the microscope. The system used in this work has the following modules:

- ES001-2.0 Emispec Vision Base Data Acquisition System;
- ES002-2.0 Scanned Imaging Module;
- ES003-2.0 EDX Spectroscopy Module.

Five workspaces are available with this configuration. Table 3-2 summarizes the work that can be performed in each one.

Workspace	Description
Scanned Imaging	Acquires scanned images from STEM detectors
EDS Spectroscopy	Acquires scanned images and EDS spectra
EDS Spectrum Image	Acquires scanned images, EDS spectra and EDS spectrum images
EDS Spectrum Profile	Acquires scanned images, EDS spectra and EDS spectrum profiles
EDS Quantification	Performs EDS quantitative analysis

Table 3-2. Emispec workspaces available.

The software used was the ES Vision 3.1. For each workspace it provides a main window with a variety of tools, displays and control panels. Although detailed information can be obtained from the software manual, a brief description about these workspaces is presented here. Figure 3-2 shows the main window for a typical workspace which might be used for image, EDS spectrum, and spectrum profile acquisition. At the top of the main window is the toolbar containing tools for a variety of tasks such as opening and saving, selecting and editing styles, and scaling and manipulating the displays which contain data and objects. At the left side, is a shortcut bar providing direct access for other workspaces and setups. At the bottom is another toolbar which contain tools that allow the user to interact with the objects within the displays, and at the right side are the control-panels which allow the user to control data acquisition parameters. In the center of the main window is the display window divided in three panes, each showing a unique type data: an image, a spectrum and a profile.

Different control panels are used in the specific workspaces. For example, in the scanned image workspace, dwell time and resolution can be controlled. Dwell time determines the time the beam stays at each point in the scan. Resolution determines the number of points scanned by controlling the distance between adjacent points in the scan. In the EDS spectroscopy workspace, real-time information about dead-time and count-rate is provided, giving feedback to continue or stop the acquisition.

In the EDS quantification workspace, the user works in direct interaction with the Periodic Table, choosing the elements to be quantified and the type of lines will be used for quantification (K, L or M-lines). Standard or standardless quantification can be

performed. The standardless mode requires that the peaks to be quantified first be "fitted"- the process of creating a mathematical model of the peaks in the spectrum for the elements to be quantified.

Background removal is performed by selection of specific energy windows in the spectrum. Different mathematical approaches can be chosen for background removal. Power-law or polynomial approaches are available and they can be used with up to five-order models. More information about the software is provided in the following sections.

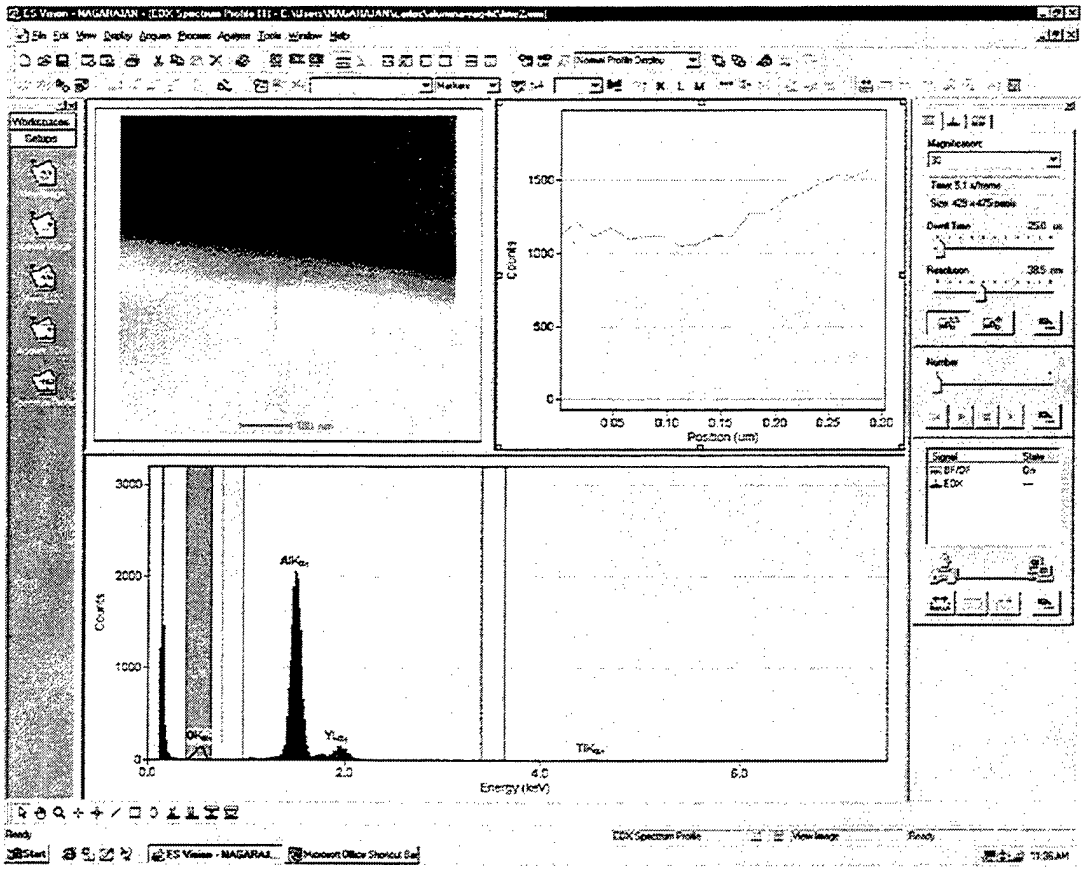

Figure 3-2. A typical window in ES Vision 3.1 for data acquisition.

B. SAMPLES

1. NiO

The NiO sample consists of a thin film of NiO deposited onto amorphous carbon and supported by a 200-mesh molybdenum grid. The NiO film thickness is ≈ 47 nm, the C film thickness is ≈ 20 nm and the Mo-grid thickness is ≈ 14 μm [Ref. 8]. The sample was acquired from SPI Supplies and it is a standard specimen used for EDS calibration and checking of AEM performance.

2. Cu-Al_2O_3

A bulk Cu-Al_2O_3 interface was created by diffusion bonding copper foils (99.999% purity) of 100 μm thick sandwiched between polished polycrystalline alumina substrates (~99.5% purity). The diffusion bonding was carried out in vacuum. The TEM sample was prepared by Mr. Richard Y. Hashimoto and a description of the sample preparation can be obtained from Ref. 9.

3. TiO_2

The TEM sample was prepared by dispersing commercial TiO_2 powder in methanol with the aid of ultrasonic agitation and pipetting the suspension onto a carbon coated copper grid and then allowed to dry at room temperature for one hour.

4. Alumina-YAG

The alumina-YAG eutectic (AYE) samples with 2.5% TiO_2 were hot pressed at 1680 °C for 15 min. in vacuum. Some of the hot pressed samples were heat treated at 1400 °C for 150 h in air. The samples were provided by Dr. Mah of UES Inc., Dayton-Ohio, for materials characterization, especially to study the Ti distribution in the AYE samples.

C. TEST PROCEDURES

1. NiO Standard Tests

The NiO sample was used to perform a series of tests to verify the work conditions of the TEM column and the EDS system. To accomplish these tests, two EDS spectra were recorded with a sample tilt of 10° using probe sizes of 9.3 and 16 nm. The probe was positioned near the center of the specimen and in the center of the grid square on which the specimen was mounted. The following tests were performed and are based on the instructions given in Ref. 8:

a. *Calibration of the Energy Scale*

The NiO sample spectrum should show characteristic peaks at energies 851 eV (Ni-Lα), 2.29 keV (Mo-Lα), 7.47 keV (Ni-Kα), 8.26 keV (Ni-Kβ) and 17.42 keV (Mo-Kα). A light element detector should also reveal peaks at 525 eV (Oxygen-K)

and 277 eV (Carbon-K). The energy axis of the EDS spectrum can be calibrated using two of the above peaks.

b. Energy Resolution

The detector energy resolution is usually defined in terms of the width of a manganese-Kα peak. However, the Ni-Kα peak is close in energy and its full width at half maximum (FWHM) can provide an estimate of the detector energy resolution: $R(Mn) \approx 0.926\ FWHM(Ni)$.

c. Peak Shape

The ratio of full width at tenth maximum (FWTM) to FWHM provides a measure of peak shape and is typically about 2.0 at the Ni-Kα (for an ideal Gaussian peak, the ratio should be 1.83). Large values may indicate peak tailing, due to incomplete charge collection.

d. Stray Electrons and X-Rays in the TEM Column

An indication of the presence of stray electrons and x-rays in the TEM column is given by the Ni-Kα/Mo-Kα count-ratio **R**(Ni/Mo):

$$\mathbf{R}(\text{Ni/Mo}) = [\mathbf{T}(\text{Ni-K}\alpha) - \mathbf{B}(\text{Ni-K}\alpha)]/[\mathbf{T}(\text{Mo-K}\alpha) - \mathbf{B}(\text{Mo-K}\alpha)] \qquad (3.1)$$

where **T** denotes the total number of counts within a 600 eV energy window centered about each peak and **B** is the sum of background counts within two 300 eV windows on

either side of the peaks. A high ratio denotes a clean column; typical values are in the range 3 to 7 for modern conventional TEMs.

e. Predominant Character of the Column Radiation

A measure of the Mo-Kα/Mo-L intensity ratio, $\mathbf{R}(Mo)_{K/L}$, making allowance for background under Mo-Kα and Mo-L peaks, gives information about the predominant character of the column radiation. If x-rays are the main source of column radiation, the ratio $\mathbf{R}(Mo)_{K/L}$ will have a high value, of the order of 100. If high-energy stray electrons are predominant, the ratio will be much lower, typically in the range of 1 to 10.

f. Total EDS Background

In addition to Bremsstrahlung x-rays produced by the incident beam, the background beneath a characteristic peak contains contributions from column x-rays and electrons outside the probe and from the EDS electronics. The peak/background ratio is a measure of the overall cleanliness of the EDS system and was defined by Fiori [Ref. 10] as the total number of characteristic counts in a particular peak divided by the number of background counts in a 10 eV region at the center of the peak. If the background **B**(Ni-Kα) is integrated over 600 eV, rather than 10 eV as specified in the definition, the peak/background ratio at the Ni-Kα peak is:

$$P/B_{10}=60[\mathbf{T}(\text{Ni-K}\alpha)-\mathbf{B}(\text{Ni-K}\alpha)]/[\mathbf{B}(\text{Ni-K}\alpha)] \qquad (3.2)$$

For 100-200 kV accelerating voltage, P/B_{10} should be at least 1000, with modern instruments giving a value closer to 3000. Low values of P/B_{10} can result from stray column radiation.

g. Check for Contamination or Icing of the Detector

For windowless and thin-window EDS detectors, the O-Kα/Ni-Kα count ratio is typically 0.2. The decreasing of this ratio with time is an indication of hydrocarbon or ice buildup on the detector or window material. The hydrocarbon and ice layers on the detector can be estimated and give an indication of the severity of the problem.

Both hydrocarbon and ice buildup on the detector, or on its protective window, will decrease the collection efficiency for Ni-Lα (870 eV) photons and increase the Ni-Kα/Ni-Lα ratio, defined by:

$$R(Ni)_{K/L} = [\mathbf{T}(\text{Ni-K}\alpha) - \mathbf{B}(\text{Ni-K}\alpha)]/[\mathbf{T}(\text{Ni-L}\alpha) - \mathbf{B}(\text{Ni-L}\alpha)] \qquad (3.3)$$

Ice is relatively ineffective at reducing the oxygen-K signal because the photon energy (525 eV) is below the oxygen K – absorption edge (535 eV). Therefore the Ni-Lα/O-K ratio, measured as:

$$R(Ni/O) = [\mathbf{T}(\text{Ni-K}\alpha) - \mathbf{B}(\text{Ni-K}\alpha)]/\mathbf{T}(\text{O–K}) - \mathbf{B}(\text{O–K})] \qquad (3.4)$$

is more affected by carbonaceous layers. If $R_0(Ni)_{K/L}$ and $R_0(Ni/O)$ are the values of these ratios measured for a clean detector (soon after installation or after thermal treatment of the detector), while $R_t(Ni)_{K/L}$ and $R_t(Ni/O)$ are the values measured when ice

and/or carbon contamination is present, the thickness **t**[ice] and **t**[C] of ice and carbon are given in nm by:

$$\mathbf{t}[\text{ice}] \approx 1850 \ln[R_t(Ni)_{K/L})/ R_0(Ni)_{K/L})] - 532 \ln[R_t(Ni/O)/R_0(Ni/O)] \quad (3.5)$$

$$\mathbf{t}[C] \approx 485 \ln[R_t(Ni/O)/R_0(Ni/O)] - 87 \ln[R_t(Ni)_{K/L}/ R_0(Ni)_{K/L}] \quad (3.6)$$

The above equations assume that the layer thicknesses are insufficient to appreciably absorb the high-energy Ni-Kα x-rays and that the hydrocarbon layer is predominantly carbon [Ref. 8].

2. Software Setup

The NiO sample was also used to define a setup for EDS quantification in the Emispec software version 3.1. Few spectra were recorded for each specimen tilt angles (zero, 5° and 10°), using a probe size of 16 nm. The zero tilt angle spectrum was recorded for 200 seconds, with a count rate of ~500 counts/sec and a dead time of 13%. The 5° tilt angle spectrum was recorded for 100 seconds, with a count rate of ~1050 counts/s and dead time of 19%. The 10° tilt angle spectra was recorded for 180 seconds, with a count rate of ~780 counts/s and dead time of 16%.

3. EDS Quantification

Verification of the defined setup and the capability to the Emispec system to perform quantitative analysis was done using the following samples: Cu-Al_2O_3, TiO_2 powder and Alumina-YAG.

Spectra from the Alumina region of the Cu-Al_2O_3 sample were recorded for specimen tilt angles of zero, 5°, 10° and 15°. Probe sizes of 9.3 and 16 nm were used. Spectra from the TiO_2 sample were recorded for tilt angles of zero and 10°, using a probe size of 16 nm. Spectra from the Alumina-YAG samples were also recorded for tilt angles of zero and 10°, but with probe sizes of 6, 9.3 and 16 nm.

4. Alumina-YAG Spectrum Profile

In order to verify the performance of the Emispec system for spectrum profile acquisition, a few line profiles were recorded across an Alumina-YAG interface from the Alumina-YAG (ht) sample. The aim is to obtain the Ti distribution across the interface and also quantify the amount of Ti in alumina, YAG and at the interface. For line profile quantification, a line profile with a length of 0.34 μm was taken for analysis. The probe size used was 16 nm and the dwell time at each point was 100 seconds. Spectra from 21 points with a spacing of 16 nm were recorded.

IV. RESULTS AND ANALYSIS

A. NiO STANDARD TESTS

The NiO standard tests were based on two EDS spectra recorded with a sample tilt angle of 10° and probe sizes of 9.3 and 16 nm. Both spectra exhibited characteristic peaks at the specific energies as expected and calibration of the energy scale was not needed. Figure 4-1 shows a bright-field STEM image of the NiO sample acquired with the Emispec system and Figure 4-2 shows the EDS spectrum recorded with the 16 nm probe size.

The average detector energy resolution, estimated using the FWHM of the Ni-Kα peak as reference, was 153.5 eV at the Mn-Kα line. The same resolution was obtained using the Emispec software. A typical energy resolution for a 10 mm^2 Si(Li) detector is 140 eV. As cited in Ref. 3, 30 mm^2 Si(Li) detectors can have resolutions that are 5 eV larger and when the resolution is measured on the microscope, there may be a further degradation, which means that the value obtained is close to the predicted value.

The ratio of FWTM/FWHM at the Ni-Kα peak was found to be 1.84, showing that the peak shape is very close to an ideal Gaussian peak. Figure 4-3 shows the Ni-Kα peak shape obtained with the 16 nm probe size.

The Ni-Kα/Mo-Kα count ratio defined by equation 3.1 was found to be ~1.2, which is an indication of stray radiation in the TEM column. However the Mo-Kα/ Mo-L count ratio was in the range of 9.2-13.40, showing that any stray radiation is due to

uncollimated high-energy electrons rather than x-rays, which is expected when operating with intermediate accelerating voltages. In addition, the peak/background ratio defined by equation 3.2 is greater than 1,000, which denote a "clean" TEM column in respect of EDS analysis.

The O-Kα/Ni-Kα count ratio obtained for both spectra was 0.18. A typical value for thin window and windowless detectors is 0.2. This suggests that there is only a minimal buildup of ice or hydrocarbon contamination on the thin window and the detector should be clean.

Table 4-1 summarizes the results obtained.

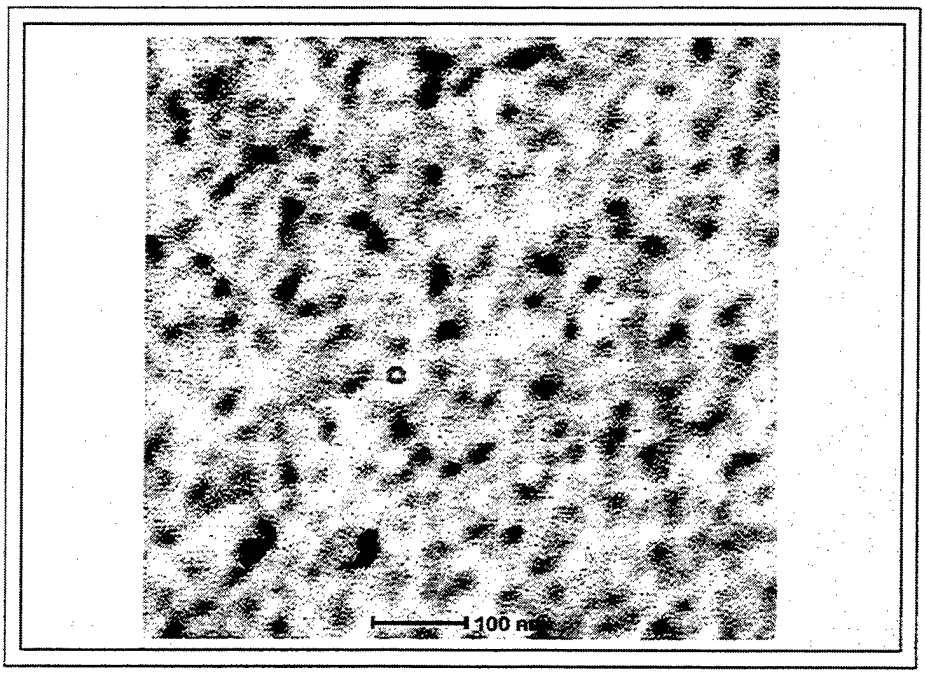

Figure 4-1. Bright field STEM micrograph of the NiO sample.

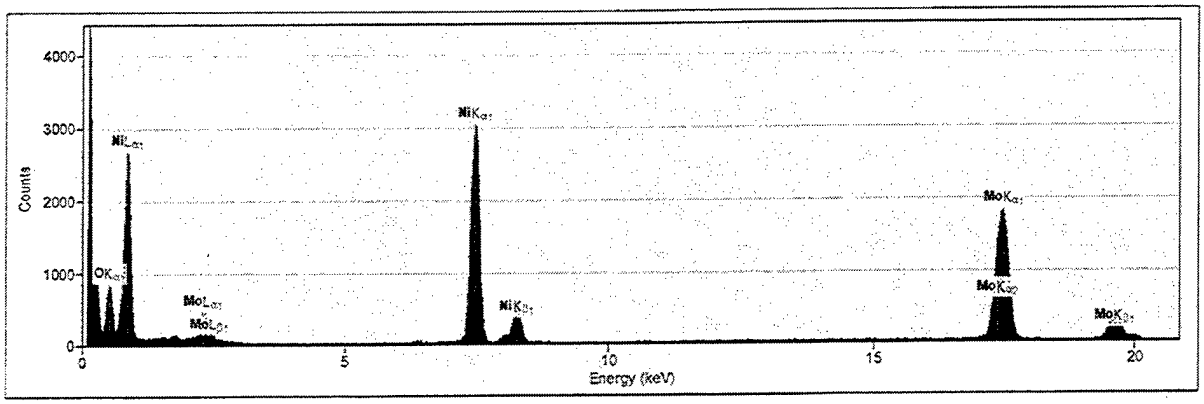

Figure 4-2. EDS spectrum of the NiO sample without background correction (10° sample tilt).

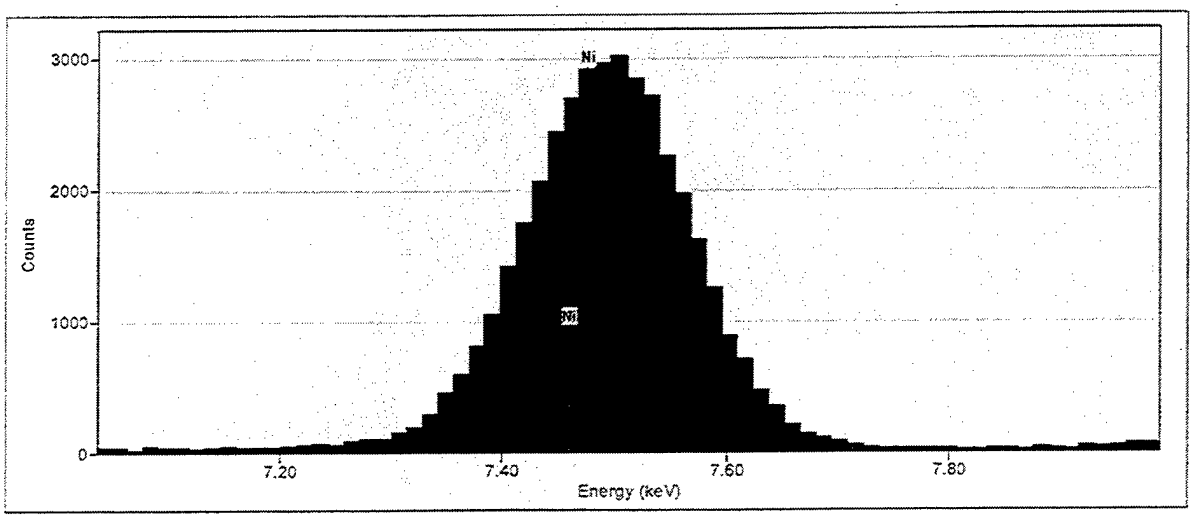

Figure 4-3. Ni-Kα peak shape.

Test	Parameter	Typical value	Experimental value	
			9.3 nm probe	16 nm probe
Energy resolution	0.926FWHM(Ni)	145 eV	153 eV	154 eV
Peak shape	FWTM/FWHM at Ni-Kα	2.0	1.84	1.84
Stray electrons and x-rays	Ni-Kα/Mo-Kα	3-7	1.21	1.23
Character of column radiation	Mo-Kα/Mo-L	1-10 (for high-energy stray electrons)	9.2	13.4
Total EDS background	P/B_{10}(Ni-Kα)	≥ 1,000	1,247	1,081
Detector contamination or icing	O-Kα/Ni-Kα	0.2	0.18	0.18

Table 4-1. NiO standard tests summary.

B. SOFTWARE SETUP

The definition of a setup for quantitative EDS analysis using the Emispec software ES Vision 3.1 was based on the results of quantitative analysis (standardless mode) performed with NiO spectra recorded with three different specimen tilt angles.

The setup requires information about the specimen, detector, microscope, fitting parameters, quantification modes and geometry of the TEM/EDS detector interface. Information about the geometry of the TEM/EDS detector interface was obtained from Refs. 7 & 10. Figure 4-4 shows a schematic of the detector-specimen stage interface. The detector angle α is the angle between the specimen surface (at 0° tilt) and a line to the center of the detector. Specimen height is the distance between the specimen surface (at 0° tilt) and the upper objective pole piece. The composition and density of the detector window were estimated by a proportional average based on the layer thickness of aluminum and polymer.

Due to the fact that the Emispec software allows the selection of various fitting and quantification parameters, many setup configurations were tried. Table 4-2 presents the setup that provided the best results for the NiO sample and was used in the subsequent quantification tests except for the information specific to each sample (thickness and density) and each test (probe size and tilt angle). Figure 4-5 shows that a good fitting was obtained by this setup. The dash line over the Ni-Kα peak represents the fitting line.

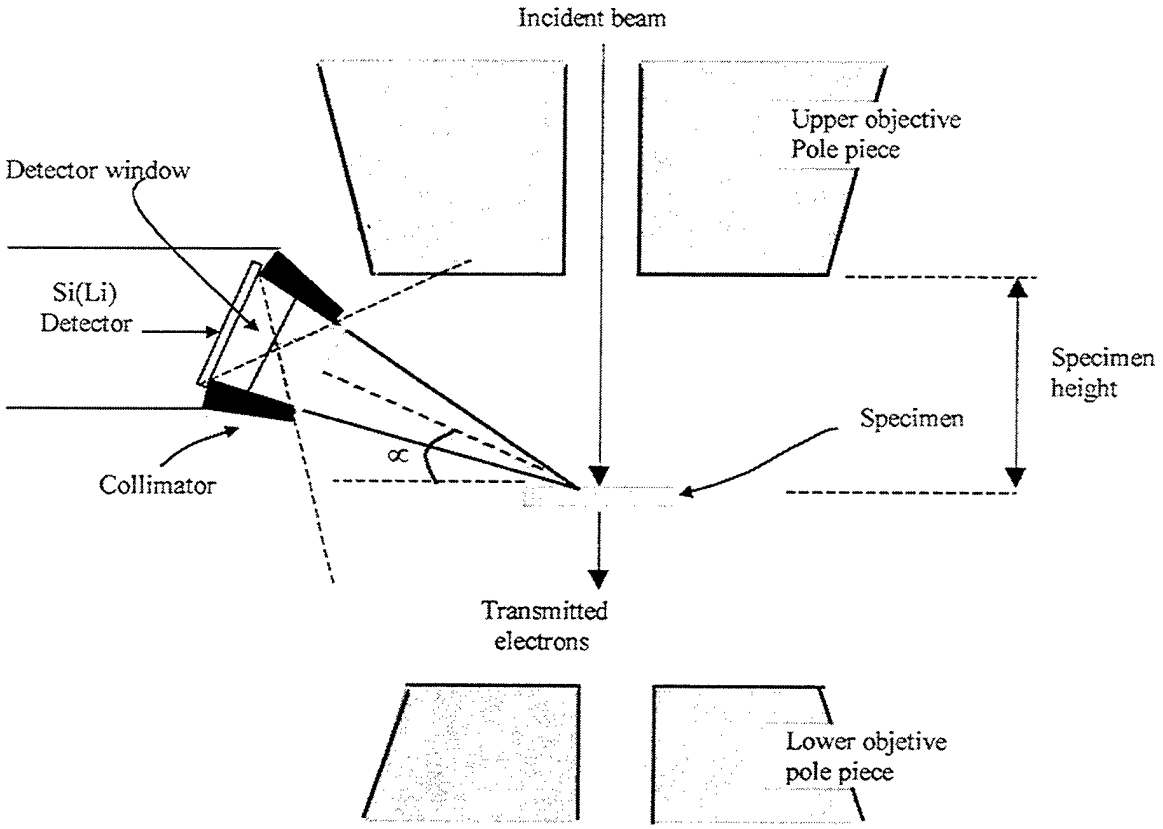

Figure 4-4. Detector-specimen stage interface.

Specimen Specimen type: Thin foil Thickness: 67 nm Density: 6.7 g/cm^3
Detector Resolution Energy resolution : 139.5 eV Reference energy: 5.9 keV Window Thickness: 0.34 nm Density: 1.57 g/cm^3 Composition (wt%): H – 2.50 C – 54.85 N – 5.81 O – 16.62 Al – 20.22 Detector Dead layer thickness: 85 nm Detector thickness: 3 mm
Microscope Type TEM Beam Accelerating voltage: 200 keV Beam current: 100 nA Beam diameter: 16 nm
Geometry Specimen Specimen height: 2.7 nm Specimen tilt 1: 0 deg Specimen tilt 2: 0 deg Detector Detector distance: 11.5 mm Detector area: 30 mm^2 Detector angle: 17.6 deg Detector azimuth: 0 deg

Table 4-2. Software setup.

Fitting Parameters Fitting width: 150% Minimum signal to noise ratio: 4 Minimum peak separation: 25% Variables (✓) Vary energy calibration (✓) Vary energy resolution Peak selection (✓) Fit all lines independently ( ) Fit alpha lines only ( ) Keep line ratios fixed
Quantification Type Standardless Acquisition Integration time: 1 sec. Analyze (✓) Normalize Correction Thickness (✓) Use alpha lines only

Table 4-2 (Cont.). Software setup

(Items with a check mark represent a selected feature).

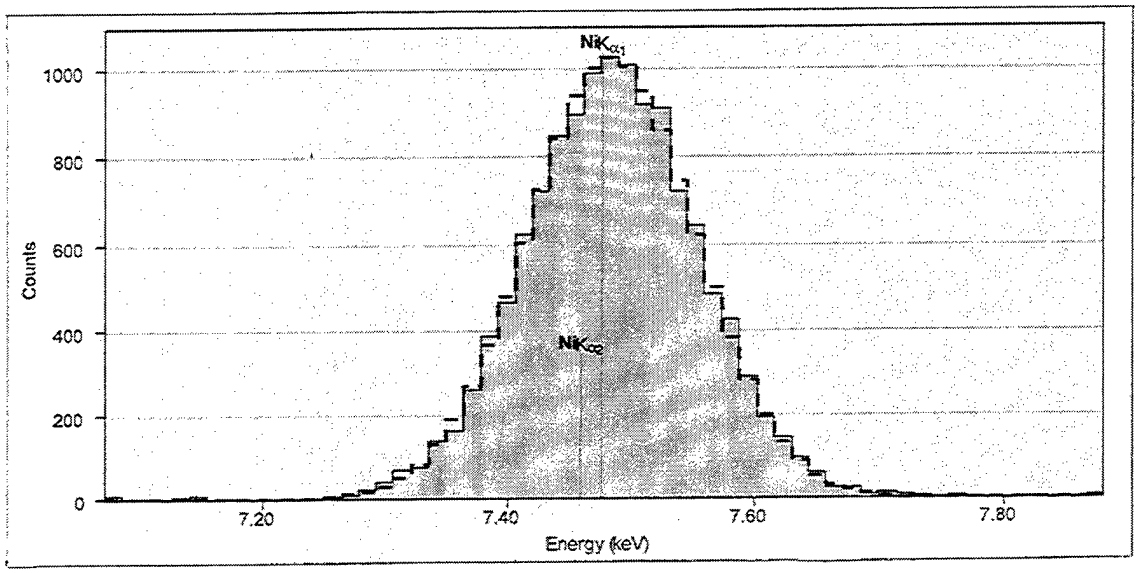

Figure 4-5. Ni-Kα peak fitting.

Some fitting setup parameters can affect the results significantly. However, changes in the peak selection mode caused only a maximum of 0.5 at.% change in the elemental composition and can be used to refine the results. Table 4-3 shows the variation in the elemental composition of a NiO sample (spectrum recorded at zero tilt angle) due to changes in the peak selection mode. Quantification results of the NiO sample as a function of the specimen tilt angle are presented in the next section.

Peak selection mode	**Ni (at.%)**	**O (at.%)**
Fit all lines independently	50.04	49.96
Fit alpha lines only	49.94	50.06
Keep line ratios fixed	49.63	50.37

Table 4-3. Changes in EDS quantification results of the NiO sample (zero tilt-angle) with the peak selection mode.

To verify which mathematical approach provides the best results for background removal, a series of quantification tests was performed using the setup defined on Table 4-2 and the NiO spectra recorded for zero tilt angle. Table 4-4 shows the results obtained. Power law 2^{nd} order was the one provided the most accurate results for the NiO sample. However, power law 1^{st} and 3^{rd} order and polynomial 2^{nd} order also provided very good

results. The width of the energy windows selected for background removal was ~1.2 FWHM of the nearest peaks, as suggested by Williams & Carter [Ref. 3]. Different widths were also tried. However 1.2 FWHM provided the best results and is used in all subsequent quantification tests.

Mathematical approach	**Ni (at.%)**	**O (at.%)**
Power Law 1st order	50.11	49.89
Power Law 2nd order	50.04	49.96
Power Law 3rd order	50.23	49.77
Polynomial 1st order	43.17	56.83
Polynomial 2nd order	50.40	49.60
Polynomial 3rd order	51.67	48.33

Table 4-4. Changes in EDS quantification results of the NiO sample (zero tilt-angle) with the background removal mathematical approach.

C. EDS QUANTIFICATION

1. NiO

Table 4-5 presents the composition of the NiO sample obtained from spectra with different specimen tilt angles. Quantification was performed using the standardless mode and the setup defined on Table 4-2. Only the K lines were selected for quantification. For zero tilt-angle, the expected composition (50 at.% Ni and 50 at.% O) was obtained, but for 5° and 10° quantification results presented a difference of ~ 6 at.%, between observed and expected values. Williams and Carter [Ref. 3] recommend operation as close to zero tilt as possible to minimize the effects of scattered radiation, which can introduce errors in quantification analysis. Tilting the specimen may increase spurious x-rays and also lowers the P/B (peak-to-background) ratio in the spectrum [Ref. 3]. In addition, absorption corrections become inaccurate because the specimen thickness is now not really definable with respect to the direction of the incident beam. In fact, almost all EDS analysis software for TEM assumes a parallel sided equithick sample with the defined thickness direction parallel to the electron beam direction.

Figures 4-6 and 4-7 shows the EDS spectra recorded with the specimen at zero tilt angle without and with background removal, respectively. Background removal was performed using the power law 2^{nd} order approximation. Figure 4-8 shows the output information of the quantitative analysis for zero tilt angle provided by the Emispec software.

Specimen tilt-angle (deg)	Ni (at. %)	O (at. %)
0	50.04	49.96
5	44.03	55.97
10	43.91	56.09

Table 4-5. EDS quantification results of the NiO sample.

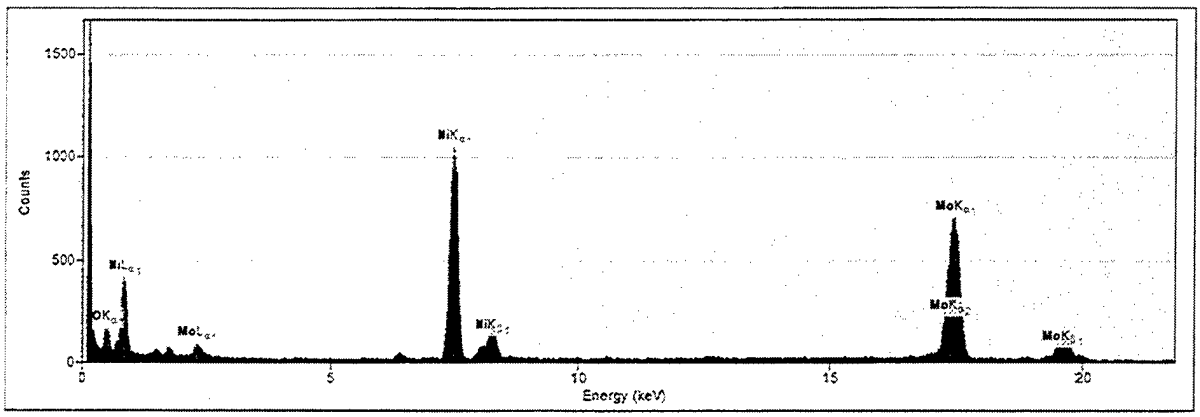

Figure 4-6. EDS spectrum of the NiO sample (zero tilt angle) without background removal.

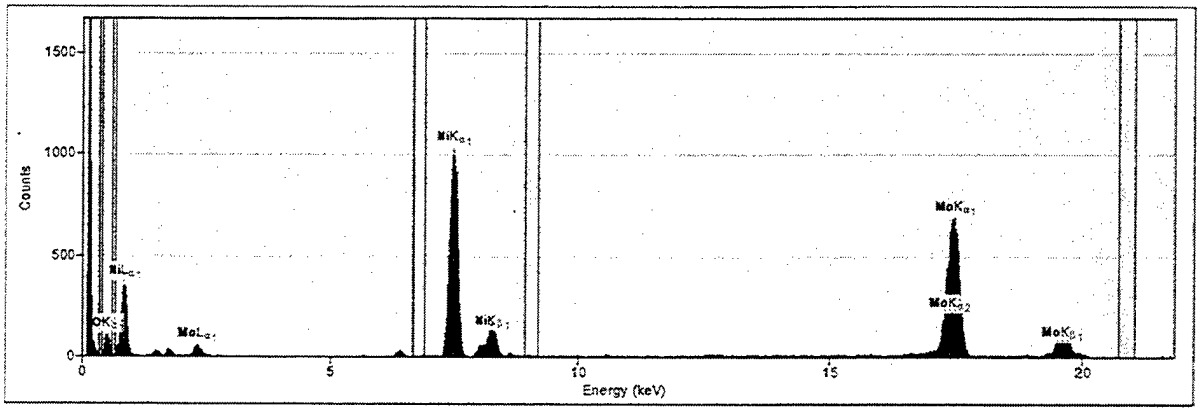

Figure 4-7. EDS spectrum of the NiO sample (zero tilt angle) with background removal.

Spectrum: NiO
Peak Intensities

O:	Ka1	933	Counts
Ni:	Ka1	12683	Counts
	Kb1	2027	Counts

Goodness of Fit
Reduced Chi Squared: 0.0060
Calibration
Channel offset: 0.0621 keV at channel 0
Channel width: 14.01 eV

Energy Resolution
Resolution: 151 eV at energy 5.900 keV

Setup
Name: Normal

Microscope Info	
Accelerating Voltage:	200.0 keV
Beam Current:	100.0 nA
Beam Diameter:	16.0 nm
EDX Detector Info	
Resolution:	139.5 eV (at 5.9 keV)
Window Thickness:	0.3 um
Window Density:	1.6 g/cm3
Dead Layer Thickness:	85.0 nm
Detector Thickness:	3.0 mm
Specimen Info	
Thickness:	67.0 nm
Density:	6.7 g/cm3
Geometry Info	
Specimen Height:	2.7 mm
Specimen Tilt 1:	0.0 deg
Specimen Tilt 2:	0.0 deg
Detector Distance:	11.5 mm
Detector Area:	30.0 mm2
Detector Azimuth:	0.0 deg
Detector Angle:	17.6 deg

Elemental Composition

Edge	Intensity	k-factor	Weight%	Atomic%	DetEff	Abs
O Ka	943	1.932	21.29%	49.96%	0.510	0.339
Ni Ka	12718	1.528	78.71%	50.04%	0.998	0.984

Total: 100.00 wt% 100.00 at%

Figure 4-8. EDS results from the NiO sample (zero tilt angle).

2. $Cu\text{-}Al_2O_3$

As mentioned previously, spectra from the alumina region of the $Cu\text{-}Al_2O_3$ sample were acquired for specimen tilt angles of zero, 5°, 10° and 15°. For zero tilt, 9.3 and 16 nm probe sizes were used. Since the thickness of this sample is unknown, quantitative analysis for different thickness were tried with the zero tilt spectrum. A thickness of 100 nm was obtained when the standardless quantification software routine gave a composition O-60 at.% and Al-40 at.% for the spectrum recorded with the 9.3 nm probe. An examination of the bright-field image of Figure 4-9 from which the spectrum was obtained suggests that this value is very reasonable. This value (100 nm) was also used to analyze the data from the tilted samples. Table 4-6 presents the quantification results obtained. Background removal using the 2^{nd} order polynomial approximation provided the best results for this sample. For zero tilt-angle, a composition close to the expected values was obtained, but a difference of ~10 at.%, between observed and expected values, results as the tilt angle increases to 15°. The results also show that a 25% variation in the specimen thickness caused a maximum of 3.0 at.% change in the composition.

Figure 4-10 shows the EDS spectrum from the alumina region of the $Cu\text{-}Al_2O_3$ sample and Figure 4-11 is the quantification results obtained for a probe size of 9.3 nm and zero tilt angle.

Specimen tilt-angle (deg)	Specimen thickness (nm)	Probe size (nm)	O (at.%)	Al (at.%)
0	100	9.3	60.03	39.97
0	75	9.3	57.62	42.38
0	100	16	57.73	42.27
5	100	16	54.52	45.48
10	100	16	52.32	47.68
15	100	16	49.20	50.80

Table 4-6. EDS quantification results of the Cu-Al_2O_3 sample.

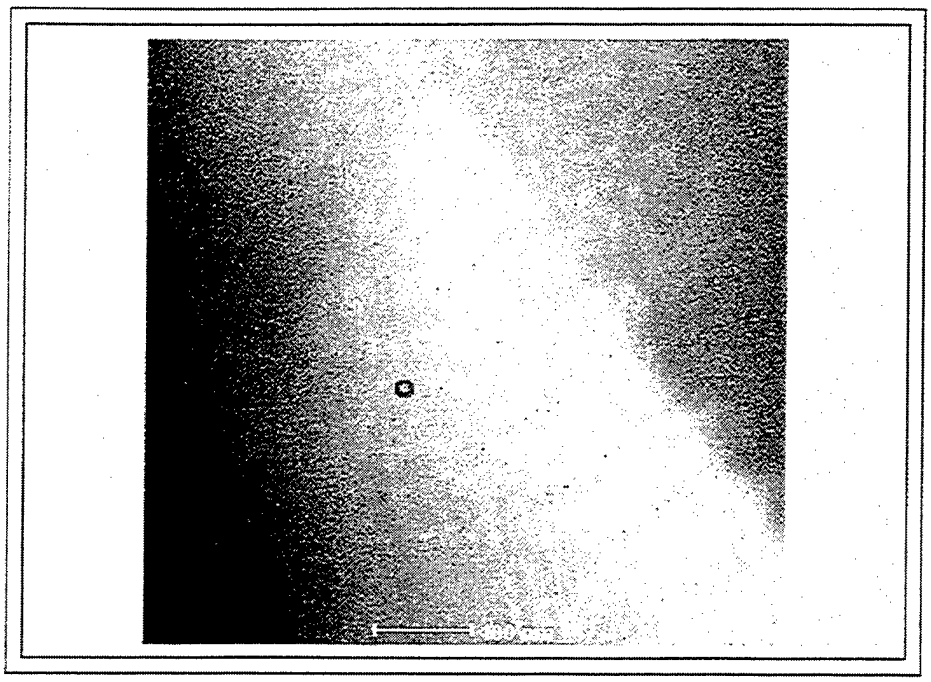

Figure 4-9. Bright field STEM image of the copper-alumina interface.

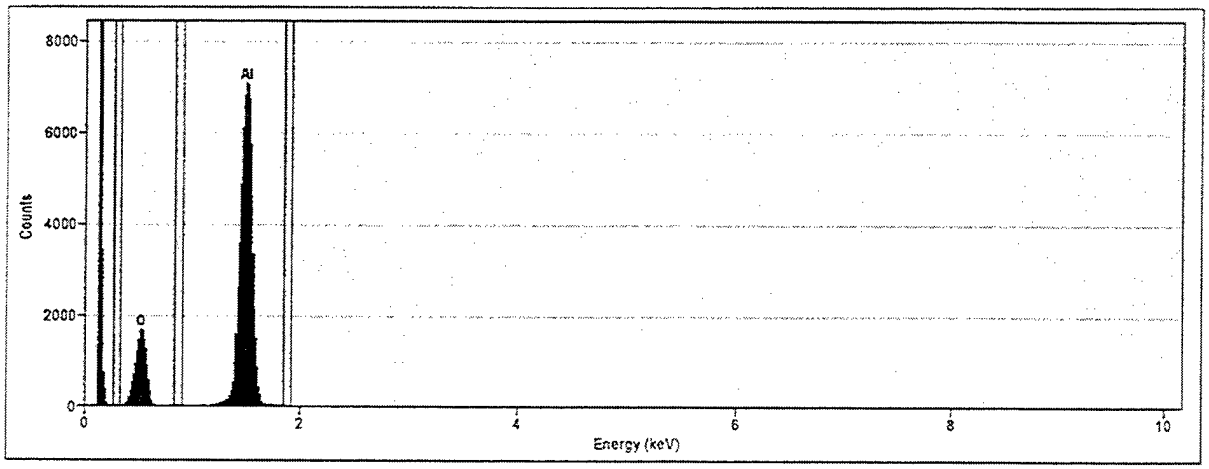

Figure 4-10. EDS spectrum taken from the alumina region of the Cu-Al_2O_3 sample (zero tilt-angle).

Spectrum: Alumina-1

Peak Intensities

O: Ka1 16785 Counts
Al: Ka1 72445 Counts
Kb1 -293 Counts
Goodness of Fit
Reduced Chi Squared: 0.0010
Calibration
Channel offset: 0.0608 keV at channel 0
Channel width: 13.86 eV

Energy Resolution

Resolution: 151 eV at energy 5.900 keV

Setup

Name: Normal
Microscope Info

Accelerating Voltage:	200.0 keV
Beam Current:	100.0 nA
Beam Diameter:	9.3 nm

EDX Detector Info

Resolution:	139.5 eV (at 5.9 keV)
Window Thickness:	0.3 um
Window Density:	1.6 g/cm3
Dead Layer Thickness:	85.0 nm
Detector Thickness:	3.0 mm

Specimen Info

Thickness:	100.0 nm
Density:	4.0 g/cm3

Geometry Info

Specimen Height:	2.7 mm
Specimen Tilt 1:	0.0 deg
Specimen Tilt 2:	0.0 deg
Detector Distance:	11.5 mm
Detector Area:	30.0 mm2
Detector Azimuth:	0.0 deg
Detector Angle:	17.6 deg

Elemental Composition

Edge	Intensity	k-factor	Weight%	Atomic%	DetEff	Abs
O Ka	16785	1.932	47.11%	60.03%	0.510	0.390
Al Ka	72445	1.008	52.89%	39.97%	0.954	0.783

Total: 100.00 wt% 100.00 at%

Figure 4-11. EDS results from the copper-alumina sample (zero tilt-angle).

3. TiO_2

Table 4-7 presents the quantitative composition of the TiO_2 sample obtained from spectra with the specimen at zero and 10° tilt angles. Standardless quantification was performed using K lines and the correct composition was obtained for the zero tilt spectrum for a value of sample thickness of 70 nm. This value was also used to analyze the spectra from the tilted samples. For background removal, 2nd order polynomial approximation was also used. For 10° tilt angle, the results show a difference of ~5 at.% between observed and expected values with a similar trend to the Al_2O_3 data.

Figure 4-12 shows a bright-field STEM image of the sample. Figure 4-13 shows the EDS spectrum and Figure 4-14, the quantification results obtained for a probe size of 16 nm and zero tilt angle. The Cu lines in this spectrum are from the sample grid.

Probe size (nm)	Specimen Thickness (nm)	Specimen tilt-angle (deg)	O (at%)	Ti (at%)
16	70	0	66.50	33.50
16	70	10	62.20	37.80

Table 4-7. EDS quantification results of the TiO_2 sample.

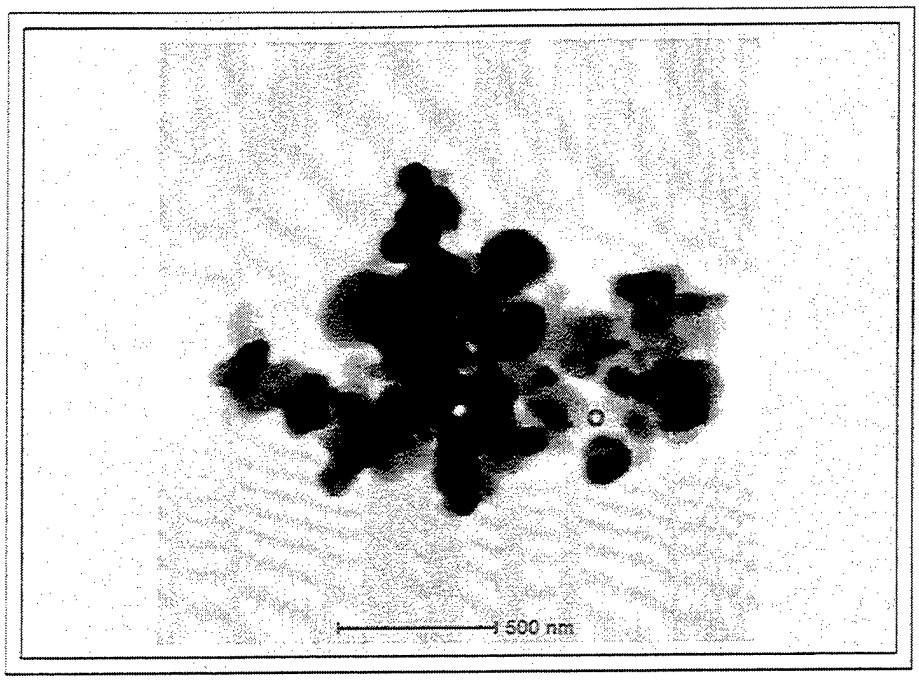

Figure 4-12. Bright field STEM image of the TiO_2 sample.

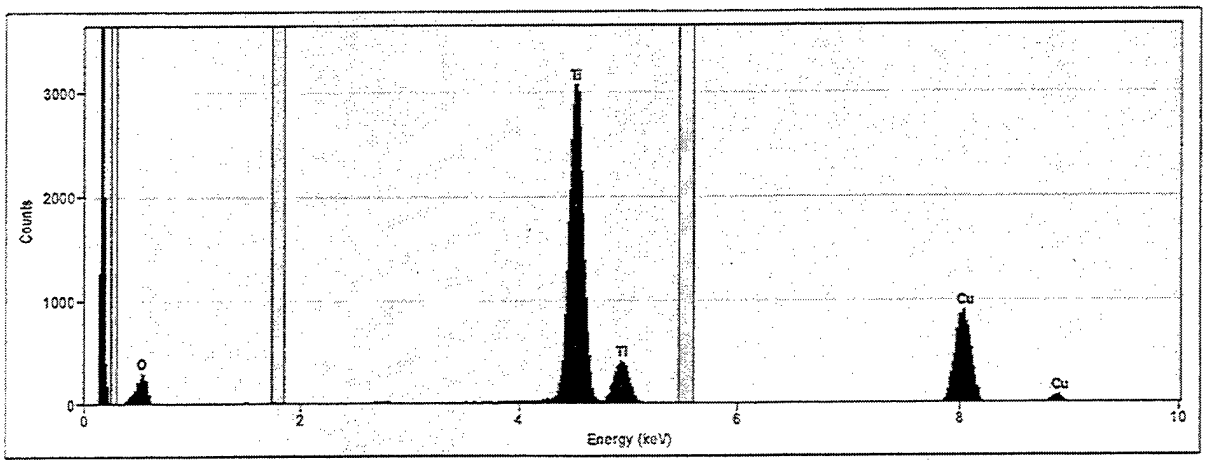

Figure 4-13. EDS spectrum of the TiO_2 sample.

Spectrum: TiO_2 test#1

Peak Intensities

```
  O:  Ka1   2637 Counts
  Ti: Ka1  35576 Counts
      Kb1   4948 Counts
Goodness of Fit
  Reduced Chi Squared: 0.0024
  Calibration
  Channel offset: 0.0684 keV at channel 0
  Channel width:  13.94 eV
```

Energy Resolution

```
  Resolution: 149 eV at energy 5.900 keV
```

Setup

```
Name: Normal
Microscope Info
Accelerating Voltage:  200.0 keV
Beam Current:          100.0 nA
Beam Diameter:          16.0 nm
EDX Detector Info
Resolution:            139.5 eV (at 5.9 keV)
Window Thickness:        0.3 um
Window Density:          1.6 g/cm3
Dead Layer Thickness:   85.0 nm
Detector Thickness:      3.0 mm
Specimen Info
Thickness:              70.0 nm
Density:                 4.3 g/cm3
Geometry Info
Specimen Height:         2.7 mm
Specimen Tilt 1:         0.0 deg
Specimen Tilt 2:         0.0 deg
Detector Distance:      11.5 mm
Detector Area:          30.0 mm2
Detector Azimuth:        0.0 deg
Detector Angle:         17.6 deg
```

Elemental Composition

Edge	Intensity	k-factor	Weight%	Atomic%	DetEff	Abs
O Ka	2637	1.932	39.87%	66.50%	0.510	0.170
Ti Ka	35576	1.248	60.13%	33.50%	0.990	0.981

Total: 100.00 wt% 100.00 at%

Figure 4-14. EDS results from the TiO_2 sample.

4. Alumina-YAG

a. Hot pressed (hp)

TEM investigation revealed the presence of three phases: Alumina, YAG and Yttrium Titanium Oxide. EDS quantification suggests that $YTiO_3$ is the composition of the latter. Figure 4-15 shows a bright-field STEM image where the existence of the three phases can be observed.

For this sample, the thickness is also unknown and a composition close to the expected values, for zero tilt angle, was obtained for a value of 100nm. This value was used to analyze all the other spectra. Table 4-8 presents the quantification results obtained. Although expected values were obtained for the alumina composition at zero tilt-angle, a difference of ~4.0 at.% was obtained in the amounts of Aluminum and Yttrium in the YAG phase. A possible reason for this difference is the slight tail overlap between the Al-Kα and Y-Lα lines which complicates the determination of their line intensities.

Figure 4-16 shows a EDS spectrum obtained from the YAG phase and the corresponding EDS analysis for this spectrum is shown in Figure 4-17. Background removal was performed using 2^{nd} order power law approximation.

b. Heat treated (ht)

TEM and EDS investigation of the heat-treated samples also showed the presence of three phases: Alumina, YAG and Yttrium Titanium Oxide. The composition

of the latter is close to Y_2TiO_5. EDS quantification also revealed the presence of small amounts of Titanium in YAG however no Ti was detected in Alumina. Table 4-9 shows the EDS quantification results. In this case the best quantification was obtained with a thickness of 150nm which seems somewhat large but not impossible. Figure 4-18 shows a bright-field STEM image of the Alumina-YAG (ht) sample and Figure 4-19, a EDS spectrum from the YAG phase.

Phase	Probe Diameter (nm)	Specimen tilt-angle (deg)	O (at %)	Al (at %)	Y (at %)	Ti (at.%)
Alumina	9.3	0	58.83	41.17	-	-
Alumina	9.3	10	48.22	51.78	-	-
Alumina	6.0	10	48.93	51.07	-	-
YAG	9.3	0	59.81	29.02	11.17	-
YAG	9.3	10	50.26	33.77	15.96	-
YAG	6.0	10	50.57	33.86	15.58	-
$YTiO_3$	16.0	10	59.28	-	22.97	17.75

Table 4-8. EDS quantification results of the Alumina-YAG (hp) sample.

Phase	Probe Diameter (nm)	Specimen tilt-angle (deg)	O (at %)	Al (at %)	Y (at %)	Ti (at.%)
Alumina	16.0	0	58.05	41.95	-	-
YAG	16.0	0	55.34	34.04	10.43	0.19
Y_2TiO_5	16.0	10	63.49	-	24.90	11.61

Table 4-9. EDS quantification results of the Alumina-YAG (ht) sample.

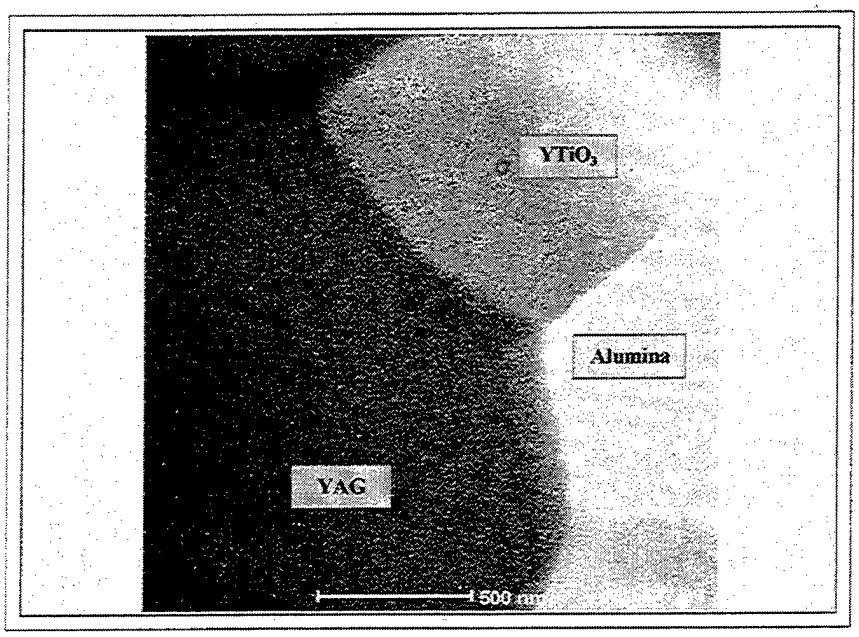

Figure 4-15. Bright field STEM image of the alumina-YAG (hp) sample.

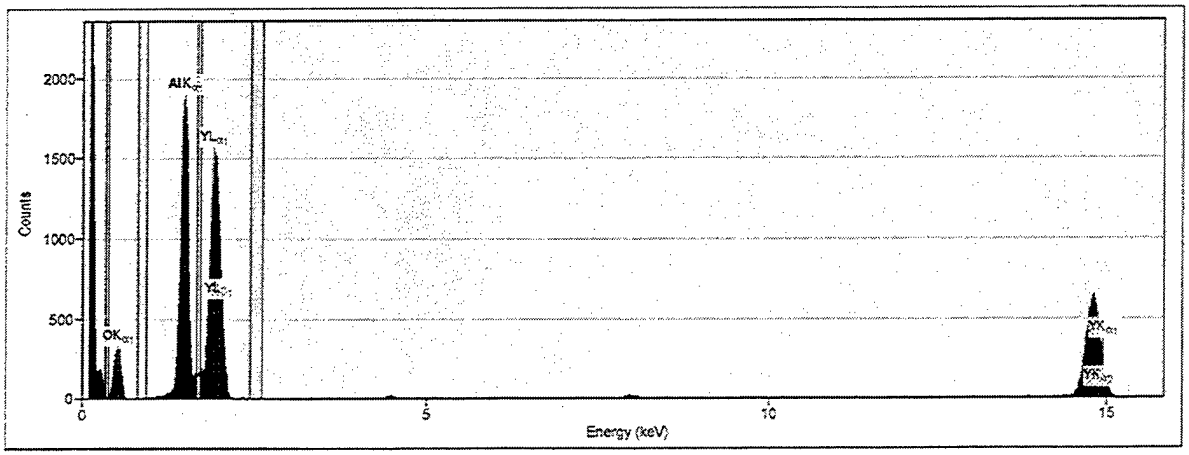

Figure 4-16. EDS spectrum taken from the YAG region of the alumina-YAG (hp) sample.

Spectrum: Alumina-YAG (hp) test# Yag-3
Peak Intensities

O:	Ka1	3275	Counts
Al:	Ka1	17748	Counts
	Kb1	2987	Counts
Y:	Ka1	5747	Counts
	Ka2	3768	Counts
	Kb1	1514	Counts
	Kb2	132	Counts

Goodness of Fit
  Reduced Chi Squared: 0.0039
Calibration
  Channel offset: 0.0497 keV at channel 0
  Channel width: 14.04 eV
Energy Resolution
  Resolution: 146 eV at energy 5.900 keV
Setup
Name: Normal

Microscope Info		
Accelerating Voltage:	200.0	keV
Beam Current:	100.0	nA
Beam Diameter:	9.3	nm
EDX Detector Info		
Resolution:	139.5	eV (at 5.9 keV)
Window Thickness:	0.3	um
Window Density:	1.6	g/cm3
Dead Layer Thickness:	85.0	nm
Detector Thickness:	3.0	mm
Specimen Info		
Thickness:	100.0	nm
Density:	4.6	g/cm3
Geometry Info		
Specimen Height:	2.7	mm
Specimen Tilt 1:	0.0	deg
Specimen Tilt 2:	0.0	deg
Detector Distance:	11.5	mm
Detector Area:	30.0	mm2
Detector Azimuth:	0.0	deg
Detector Angle:	17.6	deg

Elemental Composition

Edge	Intensity	k-factor	Weight%	Atomic%	DetEff	Abs
O Ka	3275	1.932*	35.01%	59.81%	0.510	0.197
Al Ka	17748	1.008*	28.66%	29.03%	0.954	0.681
Y Ka	9515	3.503*	36.33%	11.17%	1.000	1.000
Total:	100.00 wt%		100.00 at%			

Figure 4-17. EDS results from the alumina-YAG (hp) sample.

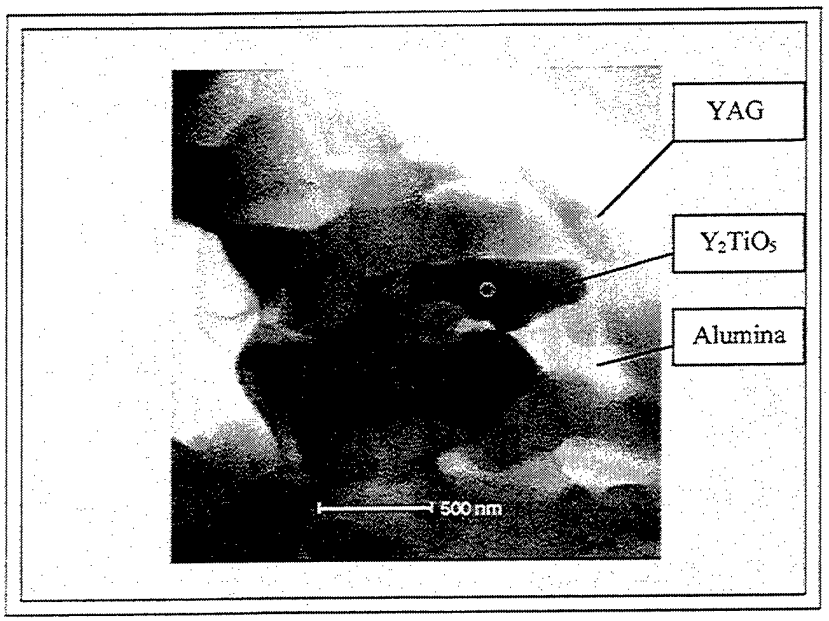

Figure 4-18. Bright field STEM image of the alumina-YAG (ht) sample.

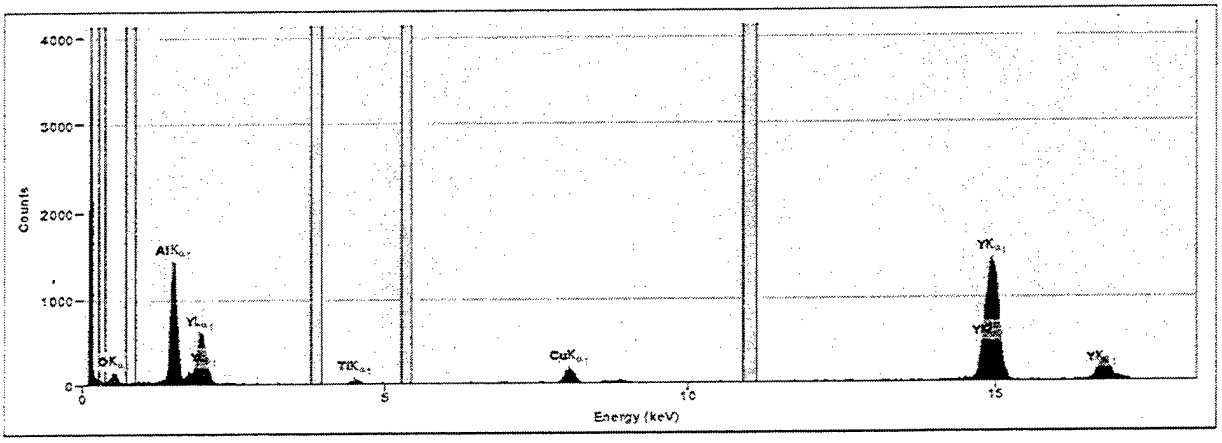

Figure 4-19. EDS spectrum taken from the YAG region of the alumina-YAG (ht) sample.

D. ALUMINA-YAG SPECTRUM PROFILE

As previously mentioned, a few line profiles were recorded across the alumina-YAG interfaces from the heat-treated samples in order to verify the performance of the Emispec system for spectrum profile acquisition. Also, the distribution of Ti across the interface was determined in the AYE heat-treated samples. Figure 4-20 is the STEM image of the alumina-YAG interface. The line marked is where the line profile was obtained. Figure 4-21 is the corresponding elemental profile plotted as intensity (# of counts) versus position. The line profile length was 0.34 μm and spectra from 21 points with a 16 nm probe size were recorded.

In order to quantify the Ti distribution, EDS quantification analysis of the 21 spectra was performed. Figure 4-22 shows the distribution of Ti in at.% versus position. This graph clearly shows that: (1) The average distribution of Ti in the YAG phase is 0.3 at.%; (2) The amount of Ti increases close to the alumina-YAG interface (~0.8 at.%); (3) No Ti was observed in the alumina phase.

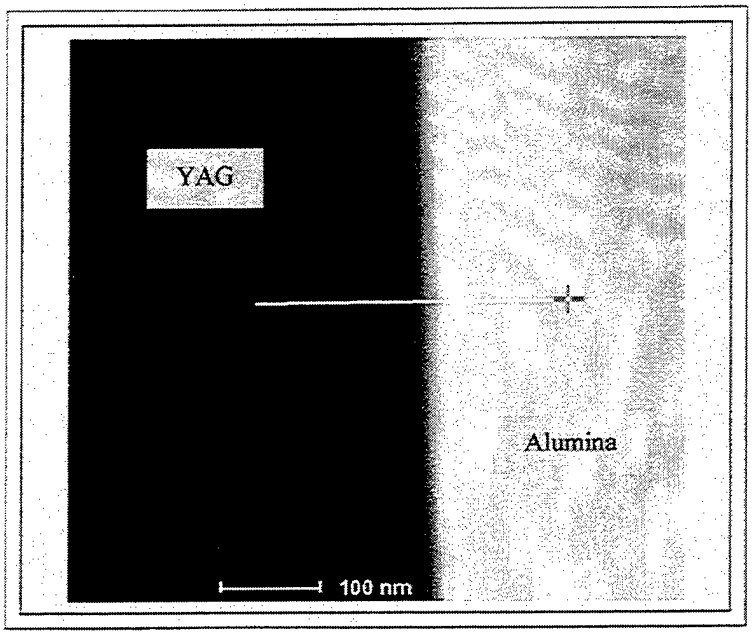

Figure 4-20. Bright field STEM image of the alumina-YAG (ht) interface.

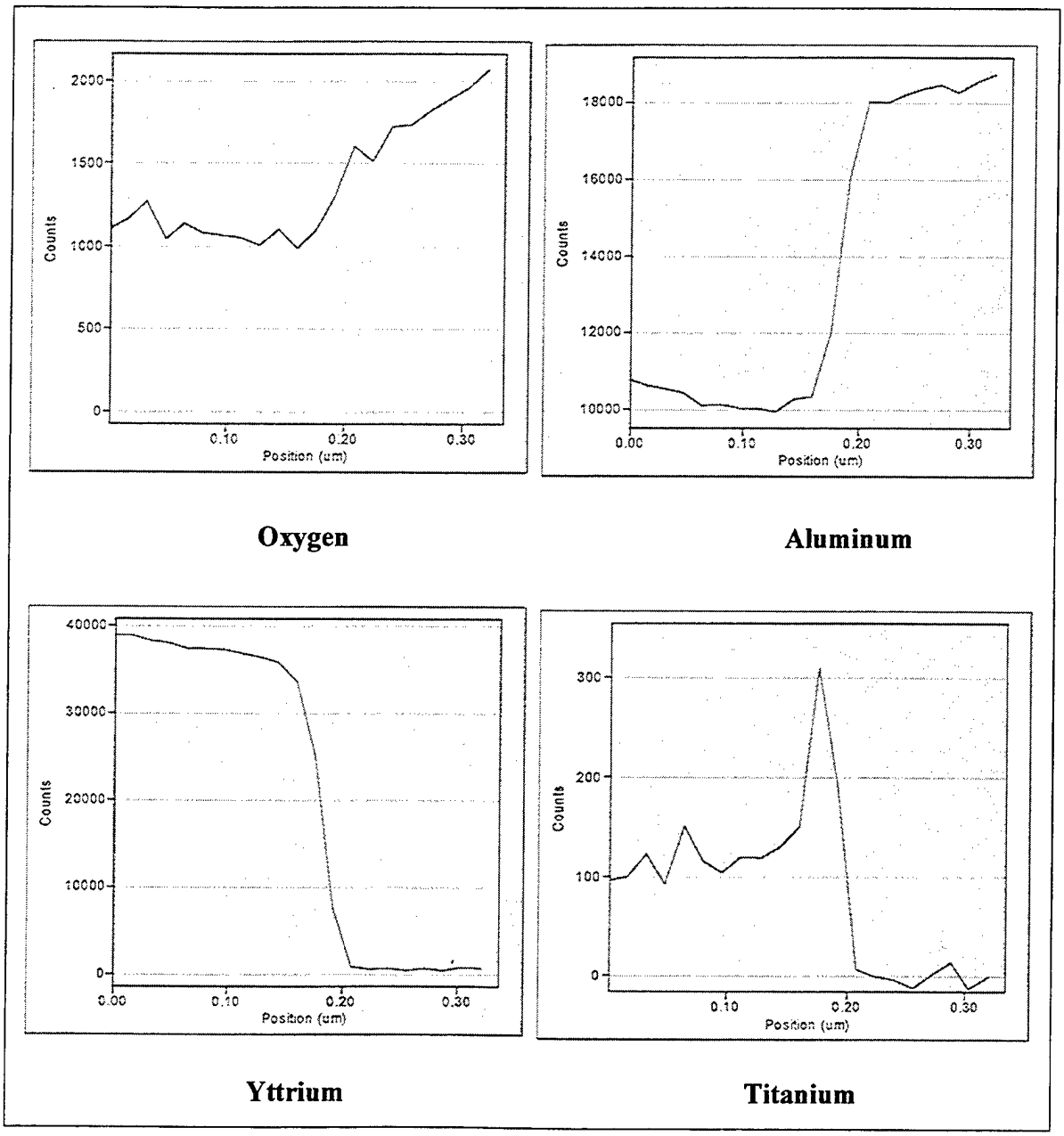

Figure 4-21. Elemental spectrum profile across the Alumina-YAG (ht) interface (The origin of the graphs is in the YAG phase).

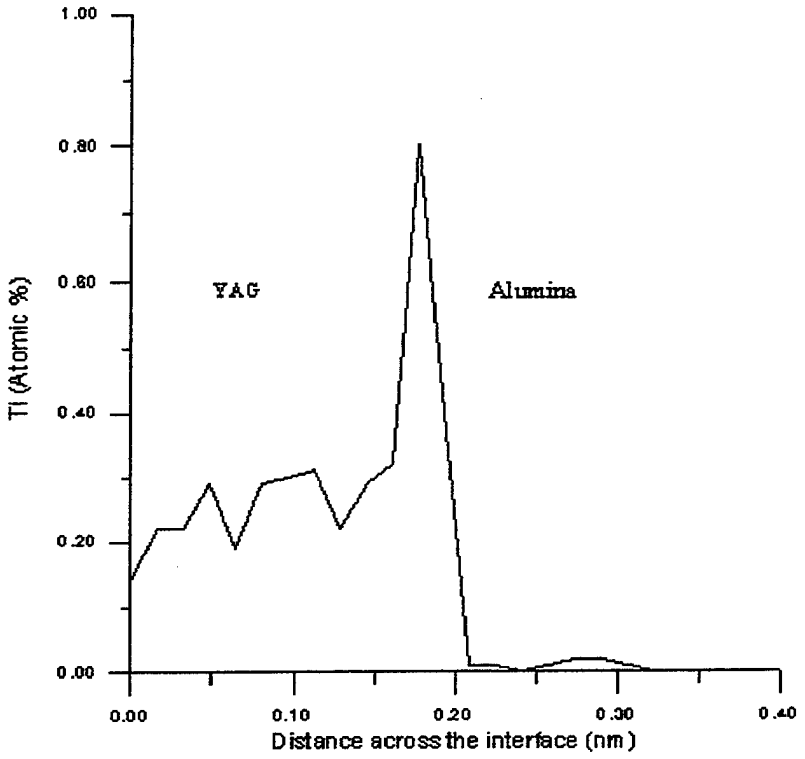

Figure 4-22. Titanium quantification profile across the alumina-YAG (ht) interface.

V. SUMMARY AND CONCLUSIONS

The NiO standard tests revealed that the Topcon 002B TEM and the EDS detector are operating in a satisfactory fashion for EDS quantitative analysis. The presence of some stray radiation was detected but the tests revealed that is due to uncollimated high-energy electrons rather than x-rays, which is normal when operating with intermediate (200-500 kV) accelerating voltage. The tests also indicated that there is only a minimal buildup of ice or hydrocarbon contamination on the detector window and this is unlikely to compromise the quality of the quantitative analysis.

An improved quantitative analysis setup configuration was developed for the Emispec software ES Vision 3.1. Accurate quantification was obtained for specimen at the zero tilt angle. Williams and Carter [Ref. 3] also suggest operation at zero tilt for quantitative analysis and the present results indicate that this is almost essential when light elements ($Z \leq 11$) are to be analyzed. Tilting the specimen may increase spurious x-rays, lower the P/B (peak-to-background) ratio in the spectrum and complicate absorption corrections because the specimen thickness cannot be really defined.

Quantitative analysis performed with TiO_2, Cu-Al_2O_3 and alumina-YAG (with 2.5% TiO_2) samples confirmed the accuracy of the new software setup if appropriate sample thicknesses were chosen.

The quantification of a line profile across an alumina-YAG interface revealed the following features of the Ti distribution at the interfaces of the alumina-YAG heat-treated samples: (1) The average distribution of Ti in the YAG phase is 0.3 at.%; (2) The amount

of Ti increases close to the alumina-YAG interface (~0.8 at.%); (3) No Ti is observed in the alumina phase.

VI. RECOMMENDATIONS

The following procedures are suggested for accurate results when performing EDS quantitative analysis with the Topcon 002B TEM and the Emispec system:

- Acquire the spectra with the specimen at zero-tilt angle;

- If possible, select only the K lines for quantification;

- For background removal select energy windows with width close to 1.2 FWHM of the nearest peaks and use 2^{nd} order power law or polynomial approximation.

The buildup of ice or hydrocarbon contamination on the detector and its window should be regularly monitored using the NiO standard sample.

LIST OF REFERENCES

1. Reimer, L., Transmission Electron Microscopy, Springer, New York, 1997.

2. Williams, David B. and Carter, C. Barry, *Transmission Electron Microscopy, Basics I*, Plenum Press, New York, 1996.

3. Williams, David B. and Carter, C. Barry, *Transmission Electron Microscopy, Spectrometry IV*, Plenum Press, New York, 1996.

4. Suryanarayana, C., Grant Norton, M., *X-Ray Diffraction, A Practical Approach,* Plenum Press, New York, 1998.

5. Keyse, R. J., and others, *Introduction to Scanning Transmission Microscopy*, Spring-Verlag, New York, 1998.

6. E-mail conversation between Mr. Andrew Nielson, Moxtek, and the author, 05 Aug 99.

7. EDAX, *DX-4 Service and Installation Manual*, New Jersey, 15 Dec 93.

8. SPI Supplies, *Instructions for Use of the SPI NiO Test Specimen.*

9. Hashimoto, R. C., *Analytical Transmission Electron Microscopy Studies on Copper-Alumina Interfaces*, Master's Thesis, Naval Postgraduate School, Monterey, California, June 1999.

10. S.M. Zemyan and D. B. Williams, "Standard Performance Criteria for Analytical Electron Microscopy", *Journal of Microscopy,* v. 174, pp. 1-14,.1994.

11. EDAX, *Drawing Part Number 9424.097.9128*, New Jersey, 22 Nov 94.